Full-Scale Bending Fatigue Tests on Stay Cables

by

Marcel Poser, Civil Engineer HTL

Thesis

Presented to the Faculty of the Graduate School of

The University of Texas at Austin

in Partial Fulfillment

of the Requirements

for the Degree of

Master of Sciences in Engineering

The University of Texas at Austin

December 2001

Full-Scale Bending Fatigue Tests on Stay Cables

Approved by
Supervising Committee:

Karl H. Frank

Sharon L. Wood

Dedication

To my parents and Hellena

for their endless support, encouragement and love.

Acknowledgements

This thesis is based on research sponsored by the Texas Department of Transportation at the Phil M. Ferguson Structural Engineering Laboratory (FSEL) at the University of Texas at Austin. I wish to express my thanks to those individuals who have been most helpful.

My appreciation goes to Dr. Karl Frank, Dr. Michael Kreger, Dr. Eric Williamson, and Dr. Sharon Wood for their suggestions, support, and advise throughout the project.

This research project required many hours of manual labor. Thank you very much to Blake Stasney, Mike Bell, and Dennis Fillip for their technical support and Tammer Botros, Manuel Razo, and Art Reinhardt for their strong backs during the specimen assembly and test setup. Joey Dowd was my research partner during the first part of the project and I would like to thank him for his ideas and his friendship.

I would also like to thank all of my fellow students at the FSEL. Their companionship and willingness to help is one of the highlights FSEL.

December 2001

Abstract

Full-Scale Bending Fatigue Tests on Stay Cables

Marcel Poser, M. S. E.

The University of Texas at Austin, 2001

Supervisors: Karl H. Frank, Sharon L. Wood

Large-amplitude stay cable vibrations caused by light rain and relatively low winds have been observed in the past few years on numerous bridges around the world. Both long-span cable-stayed bridges in Texas, the Veterans Memorial Bridge near Port Arthur and the Fred Hartman Bridge near Houston, have experienced these wind and rain induced vibrations. Full-scale 32-ft stay cable specimens are tested in bending to determine the relationship between the cable vibrations and fatigue damage. The final goal of the project is to determine the magnitude of the fatigue damage to the stay cables caused by these vibrations.

Table of Contents

List of Tables

List of Figures

CHAPTER 1
Introduction

Cable-stayed bridges have been built in rapidly increasing numbers since 1950. They are especially economical for medium to long-span bridges and are now used where previously a truss or suspension bridge might have been the first choice. Although cable-stayed bridges have many advantages, their popularity and wide usage is, according to Menn (2000), often based on prestige rather than structural efficiency or economy.

Despite the wide usage of cable-stayed bridges, there are still numerous areas of great concern, especially the stay cables themselves. One area of concern is the corrosion protection measures for the stays. The main focus is on the use of epoxy versus Portland cement grout and coated versus uncoated strand or wires. The use of high strength carbon tendons is also a topic of discussion. One of the first cable-stayed bridges in the world where carbon fibers have been used on selected tendons is the Storchenbrücke in Winterthur, Switzerland. Further topics of interest are anchorage details, behavior of in-service stay tendons, and especially the effects and elimination of cable vibration phenomenon, particularly wind and rain induced vibrations.

Wind and rain induced vibrations have been observed on numerous bridges around the world. Both long-span cable-stayed bridges in Texas, the Veterans Memorial Bridge and the Fred Hartman Bridge, have experienced wind and rain induced vibrations. Structural solutions to eliminate the cable vibrations have been studied carefully on both cable-stayed bridges. A major concern resulting from these vibrations is possible fatigue damage on the parallel seven-wire strand in the cables. The knowledge of the fatigue behavior of stay cables

subjected to out-of-plane vibrations is basically nonexistent. The fatigue behavior of stay cables under axial load is established and numerous axial fatigue tests, especially on anchorages, have been performed. However, there are still several issues regarding the long-term behavior and several corrosion issues that have not been completely resolved. It is not the intention of this thesis to discuss all the open issues regarding the fatigue behavior of stay cables. The main focus of this thesis is on full-scale bending fatigue tests of parallel seven-wire stay strand cables, identical to the ones on the Fred Hartman Bridge. The full-scale tests are part of a joint research project dealing with several issues regarding stay cable vibrations, sponsored by the Texas Department of Transportation.

In this chapter, a historical review of cable-stayed bridges, visual observation on the Fred Hartman Bridge, repairs and evaluation, as well as a review of vibration mechanisms, and the axial fatigue behavior of seven-wire strands, which are used on the Fred Hartman Bridge, are reviewed.

The following chapters present details of the stay cables of the Fred Hartman Bridge, the test setup and the test specimen preparation for the full-scale bending fatigue test, as well as test results from two full-scale tests.

1.1 HISTORY OF CABLE-STAYED BRIDGES

The idea to support a bridge deck with cables from one or two pylons has been known for a long time. The principal of cable-stayed bridges can be tracked back to the early 1600's when the Venetian Verantius built a wooden bridge supported with chain stays. In 1784 the Swiss carpenter C. J. Löscher designed a cable-stayed bridge with roughly 100 ft (30 m) span length where the entire bridge was made out of wood, including the stays (Figure 1-1).

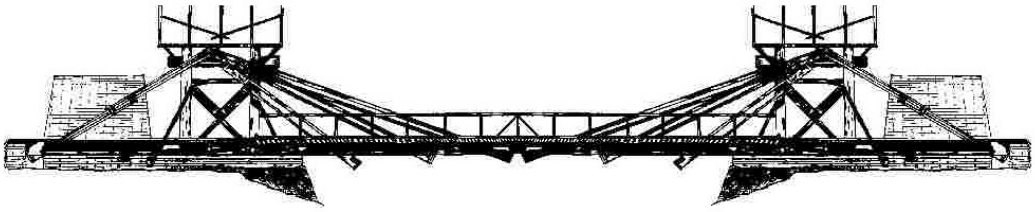

Figure 1-1: Early Design of a Cable-Stayed Bridge

In the 19th century, the French engineer Navier studied several bridge systems supported by wrought iron chains. The results of his studies show that suspension bridges should in general be preferred over cable-stayed systems. From today's point of view, it can be said with certainty that Navier's final conclusions were wrong. However, at the time Navier was studying these different bridge systems, the knowledge and equipment to achieve an even distribution of the load between all the cables, which is one of the key issues for cable-stayed bridges, was not available.

German engineers pioneered the design of cable-stayed bridges after World War II. The German engineers were challenged to find new, innovative, and inexpensive bridge designs to replace most of the Rhine river crossings which were destroyed during World War II. Dischinger proposed systems where the central span was supported by a suspension system and stay cables carried the outer parts. Dischinger's combined solutions were never adopted for an actual

bridge, but his studies had a big influence on the development of the true cable-stayed bridge system. It was not until the 1950's that Dischinger designed the first true cable-stayed bridge. The Strömsund Bridge (1955) had a main span of 599 ft (183 m) and two side spans of 245 ft (74.7 m). Gimsing (1999) attributes the increase in cable-stayed bridge designs to the improved technique of structural analysis tools that were available. The Germans further developed the design of cable-stayed bridges in the following decades and built several of them. The series of bridges near Dusiburg across the Rhine River are examples of these pioneering German bridges.

The first cable-stayed bridge in the United States was the Sitka Harbor Bridge in Alaska, which was opened to traffic in 1971. Currently, there are about 20 long-span cable-stayed bridges in service in the United States. There are two cable-stayed bridges in the inventory of the Texas Department of Transportation (TxDOT), the Veterans Memorial Bridge near Port Arthur (Figure 1-2) and the Fred Hartman Bridge across the Houston Ship Channel (Figure 1-3).

Figure 1-2: Veterans Memorial

Figure 1-3: Fred Hartman

The longest cable-stayed bridge in the 20th century was built as part of the Honshu-Shikoki Bridge Project in Japan. The Tatara Bridge has a main span of

920 ft (890 m) and was completed in 1999 (Figure 1-4). Table 1-1 shows the 10 longest cable-stayed bridges in the world.

Figure 1-4: Tatara Bridge, Japan

Table 1-1: Longest Cable-Stayed Bridges

#	Name	Country	Span [ft]	Span [m]	Year
1	Tatara	Japan	2920	890	1999
2	Pont de Normandie	France	2808	856	1995
3	Qing Zhou Min Jiang	China	1985	605	1996
4	Yangpu	China	1975	602	1993
5	Xupu	China	1936	590	1996
6	Meiko Chuo	Japan	1936	590	1997
7	Skarnsund	Norway	1739	530	1991
8	Tsurumi Tsubasa	Japan	1673	510	1995
9	Ikuchi	Japan	1608	490	1991
10	Öresund Bridge	Sweden	1608	490	1999
...					
…	Fred Hartman	USA	1250	381	1995

1.2 CONCERNS ON THE FRED HARTMAN BRIDGE

Large amplitude stay cable vibrations have been observed on the Fred Hartman Bridge numerous times since its opening in 1995. One of the first estimates of the amplitude is from visual observations during a four-day period between April 1st and April 4th 1996 shown in Table 1-2 (Poston 1998).

Table 1-2: Observed Cable Vibrations

Cable ID	Mode	Frequency	Amplitude
9	2	2.1 Hz	15 in (380 mm)
1, 2, 3	1	0.8 Hz	25 in (635 mm)
10, 11	2	> 1.5 Hz	4 in (100 mm)
15, 16	1	1.0 Hz	12 in (305 mm)
23, 24	2	1.2 Hz	26 in (660 mm)

24	3	1.8 Hz	42 in (1065 mm)

Captures of a video taken on April 4th 1997 (Figure 1-5) show the large deformations cable 24 undergoes during an event. At 650 ft (198 m), cable 24 is the longest cable on the bridge (Poston 1998).

Studies have shown that the vibrations are due to the so-called wind and rain induced vibration phenomenon, which is presented in more detail in the following paragraphs. These large amplitude vibrations caused visual damage to the Fred Hartman Bridge. Broken guide pipes, which were found on 101 of the total of 192 anchorages, are shown in Figure 1-6. The broken guide pipes are a visual indication of the forces generated by these events and the damage that might occur. Of great concern is the possible fatigue damage on the actual stay cables and the anchorage. However, it is impossible to reliably detect possible damage with nondestructive methods.

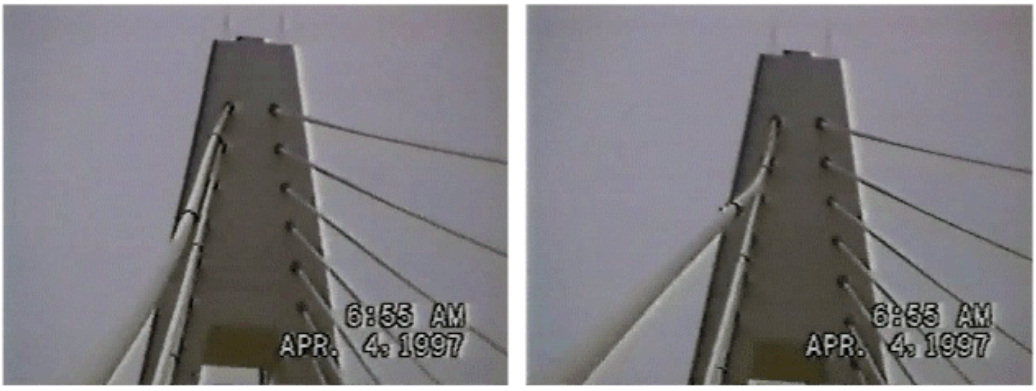

Figure 1-5: Stay Cable Vibrations

Figure 1-6: Broken Guide Pipe

1.3 REPAIR AND EVALUATION ON THE FRED HARTMAN BRIDGE

Whitlock, Dalrymple, Poston, and Associates (WDP), Johns Hopkins University, Texas Tech University, and the University of Texas at Austin (UT) have been retained by TxDOT to investigate the wind and rain induced vibration phenomenon observed on the Fred Hartman Bridge and the Veterans Memorial Bridge and to propose repairs and upgrades.

WDP is mainly concerned with the repair of existing damage and with structural solutions to eliminate the cable vibrations. The broken guide pipes were strengthened with stiffeners, which now allow the pipe to withstand the large forces due to the cable vibrations. Note that the retrofitted guide pipes do not prevent the cable vibrations. A temporary solution to control the vibrations was the installation of cable restrainers as shown in Figure 1-7. The restrainers connect the stay cables to allow vibration energy to be transferred to adjacent stays.

Figure 1-7: Cable Restrainer

Two types of dampers were designed and tested by WDP as possible methods to prevent the large amplitude vibrations. A linear damper, which is attached perpendicular to the cable (Figure 1-8) and a pressurized bladder system, developed by Freyssinet, which surrounds the cable (Figure 1-9), have been installed. The dampers have to be designed based on the characteristics of each

stay cable. Furthermore, the usage of a non-linear damper, which is a further development of the linear damper, has been discussed.

Figure 1-8: Linear Damper

Figure 1-9: Freyssinet Damper

Johns Hopkins University instrumented several cables of the Fred Hartman Bridge and the Veterans Memorial Bridge to collect vibration data and to model the vibration characteristics. It is essential to understand the vibration characteristics of each cable to be able to setup efficient dampers.

Texas Tech University is attempting to produce aerodynamic damping solutions. Their proposed solution consists of a number of rings wrapped around the cable to prevent the formation of the rainwater rivulets.

The studies at UT focus on the fatigue behavior of the stay cables of the Fred Hartman Bridge. The research program consists of three phases: field measurements on stay cables of the Fred Hartman Bridge to determine the relationship between measured strains and accelerations during an event, four full-size fatigue tests in the laboratory to determine the fatigue behavior, and the

development of analytical models of the stay cables. This thesis covers the first two of the four fatigue tests.

1.4 STAY CABLE VIBRATIONS

Numerous cable vibration mechanisms have been identified and characterized with the four most common phenomena being vortex shedding, galloping, deck – cable interaction, and wind and rain induced vibrations (Gimsing 1997 & 1999, Ito 1999, Miyazaki 1999, Virlogeux 1998). Most of these mechanisms were noted to play an important role on the Fred Hartman Bridge.

1.4.1 Vortex Shedding

Vortex shedding is essentially the phenomenon that makes a flag flutter in the wind. Airflow that is forced around an object produces vortices shedding off of the object as indicated in Figure 1-10. Consecutive vortices that shed off of opposite sides of the object produce alternating perpendicular forces. If the frequency of the alternating forces matches any of the natural frequencies of the cable, large amplitude vibrations will occur.

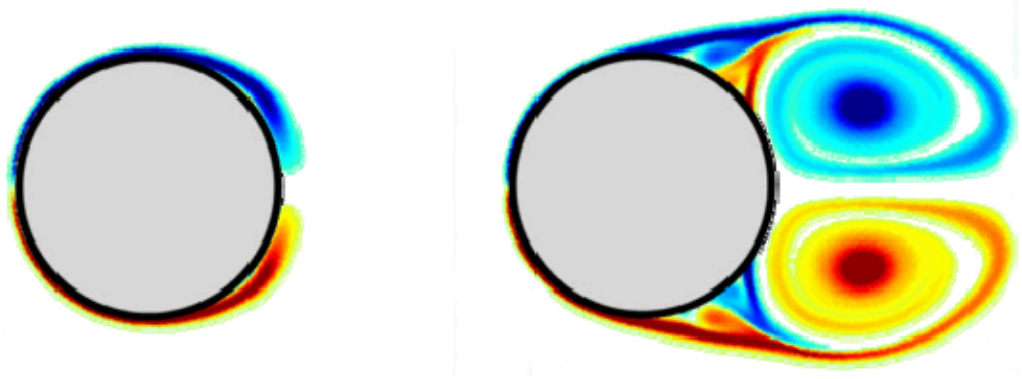

Figure 1-10: Development of Vortices

1.4.2 Galloping

Galloping is a phenomenon that occurs because of aerodynamic instability where the airflow creates uplift forces around an unsymmetrical cross section. Galloping may occur on stay cables if the airflow hits at an angle such that the effective aerodynamic shape of the cable is an elliptical cross section. In addition, formation of ice on the cable can also change the cross section of a stay cable to induce galloping perpendicular to the airflow.

1.4.3 Deck and Cable Interaction

Cable vibration can also occur because of structural vibrations of the bridge deck or the pylon, which is transferred through the anchorage into the stay cable. Deck and pylon vibration can occur because of aerodynamic effects or because of periodic traffic loads, such as trains and trucks.

1.4.4 Wind and Rain Induced Vibrations

The phenomenon that produces by far the largest amplitudes is wind and rain induced vibrations. The first time these kinds of vibrations were described and further investigated was in 1984 during the construction of the Meikonishi Bridge in Japan.

Interestingly, it was noticed that the vibrations only occur on stay cables that are covered with a smooth polyethylene pipe at relatively low wind speeds and light rain fall, giving birth to the term wind and rain induced vibrations.

The rainwater forms one or two rivulets under the influence of the airflow around the cable, which will then change the aerodynamic cross section of the stay cable in such a way that it is susceptible to vibrations (Figure 1-11). Once the cable starts vibrating, the rivulets start to oscillate at the same frequency as the cable. Interesting to note, wind and rain induced vibrations have never been reported during heavy winds. This can be explained by the fact that the rivulets get blown off the cable surface as the wind speed increases.

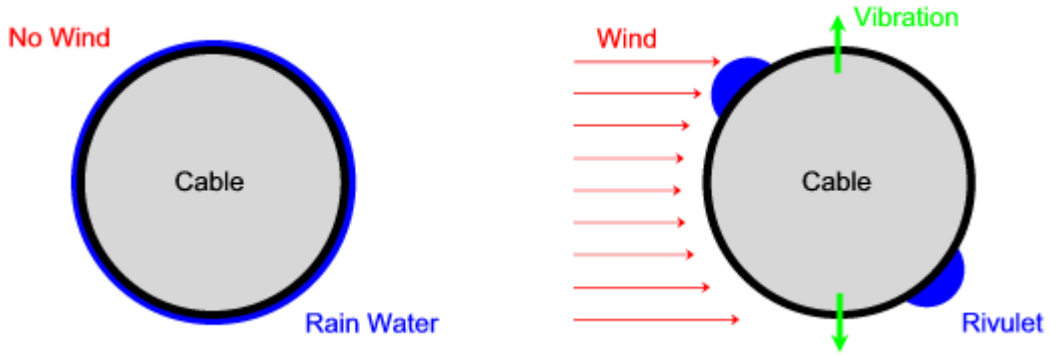

Figure 1-11: Wind-Rain Vibration Mechanism

1.4.5 Vibration Mechanisms on the Fred Hartman Bridge

Preliminary results characterized by Johns Hopkins University (Jones et al. 1999 - 2001) regarding the vibration characteristics of the cables of the Fred Hartman Bridge are summarized below.

The most common vibration mechanism observed on the Fred Hartman Bridge is probably vortex shedding. Vortex induced vibrations are normally associated with modes higher than 5^{th} mode. The displacements during these

vibration events are relatively small. However, because of the high frequencies, the acceleration amplitude might be very significant during an event.

The dominant modes during wind and rain induced vibration range from the 1st to 4th mode, with 2nd and 3rd being the predominant ones. The corresponding natural frequencies have been identified to be between 1 and 3 Hz. The observations made compare reasonably well with the observations made on other cable-stayed bridges susceptible to wind and rain vibration. It appears that every stay has a preferred mode of vibration that occurs within a wide range of wind speeds, with speeds between 16 – 42 ft/s (5 – 13 m/s) being the most critical. Wind directions also play an important role in the likelihood and amplitude of vibrations. The wind directions that resulted in the largest amplitudes have been identified to be around 60 degrees for the cables declined from the north and around 110 degrees for the cables that decline from the south. An angle of 0 degrees would correspond to the northbound direction of the bridge and an angle of 180 degrees to the southbound direction.

It was further noticed that deck vibration triggered very large amplitude cable vibration on the Fred Hartman Bridge. Deck vibration was first observed before subsequent stay cable vibrations at the same frequency. The knowledge base is currently very limited and efforts are under way to characterize this vibration phenomenon.

1.5 FATIGUE OF STAY CABLES

Over the years, numerous stay cable systems have been developed and successfully used on cable-stayed bridges. However, the most widely used system in the 20th century was the parallel-strand cable system. The system consists of a bundle of parallel seven-wire 0.6-in (15-mm) diameter strands (Table 1-3), surrounded by a polyethylene (PE) pipe, which is then grouted to protect the

strand from corrosion. This type of system is used on the Fred Hartman Bridge and the Veterans Memorial Bridge. The axial fatigue performance of strand and stays consisting of strand is reviewed in this section.

It should be noted at this point, that axial fatigue tests were intended to be anchorage performance tests. They are required for all new cable-stayed bridge in the United States. However, because numerous failures occurred outside the anchorage region, these tests provide information on the complete stay system.

Table 1-3: Technical Data of Seven-Wire 0.6-in. Strand (ASTM A416)

Grade	**270 K**	
Nominal Diameter	0.6 in	15.24 mm
Strand Tolerance	0.6102 / 0.5941 in	15.50 / 15.09 mm
Modulus of Elasticity	27500 ksi	190,000 N/mm^2
Min. Breaking Strength	58.6 kip	261 kN
Min. Yield Strength	52.74 kip	235 kN
Nominal Area	0.2170 in^2	140.00 mm^2
Nominal Weight	740 lbs/1000 ft	1,102 kg/1000 m

Note, in an axial fatigue test the entire length of the specimen is subjected to the same applied stress range. A specimen subjected to bending has only few and localized higher stresses areas, as for example at the anchorage. Therefore, the probability that an initial flaw is present in a higher stress region is much smaller in a bending fatigue test than in an axial test. Initial flaws on the strand can lead to fatigue cracks and wire fracture. However, the data on axial fatigue tests should give a general idea of the fatigue behavior of strand.

Only very few bending fatigue tests on stay cables have been performed worldwide. In the United States a small number of saddle tests have been performed. A summary of the only well-documented bending fatigue test, done in Japan, is presented although the tested specimens were not parallel strand cables.

1.5.1 Axial Fatigue Tests on Stay Cables

At the Ferguson Structural Engineering Laboratory (FSEL) axial fatigue tests have been performed on four types of cable specimens of the Fred Hartman Bridge (Frank et al. 1989). All four test specimens were 17 ft 4 in. (5.61 m) long and were tested in a large vertical force test frame.

The specimens were stressed to an initial load of 40% GUTS before grouting. After grouting, they were tensioned to the lower fatigue load level and then cycled at a constant load range for 2 million cycles at frequencies between 0.6 and 1.5 Hz. The load range for each specimen resulted in roughly the same stress range of 23 ksi (160 N/mm^2). Table 1-4 summaries the load and the strand stress ranges, assuming an even load distribution among the strands.

Table 1-4: Load and Stress Ranges of FSEL Tests

Test	**#1**	**#2**	**#3**	**#4**	
Number of Strands	19	43	55	55	
Lower Load Level	406.3	916.6	1176.2	1176.2	kip
Upper Load Level	500.9	1133.7	1450.1	1450.1	kip
Load Range (Stay)	94.6	217.1	273.9	273.9	kip
Load Range (Strand)	5.0	5.0	5.0	5.0	kip

Stress Range	**22.9**	**23.3**	**22.9**	**22.9**	**ksi**
Lower Load Level	1807.2	4077.0	5231.7	5231.7	kN
Upper Load Level	2228.0	5042.7	6450.0	6450.0	kN
Load Range (Stay)	420.8	965.7	1218.3	1218.3	kN
Load Range (Strand)	22.1	22.5	22.2	22.2	kN
Stress Range	**158.2**	**160.4**	**158.2**	**158.2**	**N/mm^2**

Wedge seating and stiffness checks were also performed before and during the fatigue test. After the fatigue test, an ultimate static test was performed. Because of the ultimate static test, it was not possible to determine whether a wire break occurred during the fatigue test or fractured from a fatigue crack. However, it was possible to tell from looking at the fracture surfaces whether the break was initiated by fatigue. In addition to the fracture surface investigation, a transducer was also used in some of the later tests to detect wire breaks.

All four tests had some fatigue cracks / wire breaks which occurred during the 2 million cycles of the fatigue test. The location and the number of fatigue cracks are summarized in Table 1-5.

Note that all four tests showed wire breaks in the top transition region and only test #2 showed wire fractures in the bottom transition region. Fifty-nine percent of the breaks occurred in the top anchorage region (Wedges and Transition Region), 26% in the free length or at contact points with the helical spacer wire in the free length, and 15% in the bottom anchorage (Wedges and Transition Region).

Table 1-5: Location of Fatigue Wire Breaks of FSEL Test

Test	**#1**	**#2**	**#3**	**#4**	**Total**	**%**

Number of Strands	19	43	55	55		
Number of Wires	**133**	**301**	**385**	**385**		
Failures at Top Wedges	3		2		**5**	**9%**
Failures in Top Transition Region	2	1	11	13	**27**	**50%**
Failures in Free Length			6		**6**	**11%**
Failures at Contact Points with Helix			8		**8**	**15%**
Failures at Bottom Transition Region		7			**7**	**13%**
Failure at Bottom Wedges			1		**1**	**2%**
Total Failures	**5**	**8**	**28**	**13**	**54**	
%	**3.8%**	**2.7%**	**7.3%**	**3.4%**		

In the autopsy of the stays, circumferential cracks were found in the grout, spaced at about 1 in. Longitudinal cracks over the entire specimen length were found above strands where wire breaks occurred. Dark corrosion spots on strands were reported on various locations along the specimen. Some tests, particularly test #3, showed heavy corrosion at the top and bottom anchor heads.

As shown in Table 1-5, none of the four specimens fulfilled the fatigue test requirement of 2% wire breaks after 2 million cycles – the recommendation of the Post-Tensioning Institute (PTI) Committee on Stay Cable Bridges. It should also be mentioned that the 55-strand specimen did not reach 95% of guaranteed ultimate tensile strength (GUTS) as shown in Table 1-6. The ultimate tensile test is a requirement in some bridge specifications.

As a result of the four tests performed at FSEL, one extra strand was added to all stay cables for the actual design of the Fred Hartman Bridge. This measure is certainly somewhat questionable.

Table 1-6: Ultimate Tensile Tests of FSEL Tests

Test	**#1**	**#2**	**#3**	**#4**	
Number of Strands	19	43	55	55	
Ultimate Tensile Test	1140	2577	3165	N/A	kip
95% of GUTS	1114	2576	3271	3271	kip
Difference	**+26**	**+1**	**-106**	**N/A**	**kip**
Ultimate Tensile Test	5071	11462	14078	N/A	kN
95% of GUTS	4955	11458	14549	14549	kN
Difference	**+ 116**	**+ 4**	**- 471**	**N/A**	**kN**

The Construction Technology Laboratories (CTL) has performed a series of full-scale axial fatigue and strength tests on stay cables with epoxy coated, as well as uncoated, seven-wire strands. The tested specimen sizes reach from 17 to 156 strands and lengths between 15 and 48 ft (4.6 m and 14.6 m). The various tests also included different anchorage systems.

CTL published a summary of the tested stays up to 1995 (Tabatabai et al. 1995). The results of the tested stays show that most cables experience wire fracture during a 2 million-cycle fatigue test with a fatigue load ranging from 36.5% to 45% of GUTS, which results in a stress range of roughly 23 ksi (160

N/mm^2) assuming an even load distribution. The percentages of broken wires after 2 million cycles vary from 0% to 27% with first breakages occurring as early as 600 cycles. Not all specimens achieved the required tensile capacity (95% GUTS) in the static test. In some tests a number of failures occurred at corroded areas of the strand.

1.5.2 Japanese Bending Fatigue Tests on Stay Cables

Probably the biggest series of full-size axial and bending fatigue tests on bridge cables was undertaken as part of the Honshu-Shikoki Bridge Project in Japan. The tests were conducted at the Japan Construction Method and Machinery Research Institute (Miki et al. 1992).

Axial fatigue was an important issue for the cable-stayed bridges on the Kojima-Sakaida route because of the large variation of the live load, combined highway and rail traffic route. Bending fatigue was of general concern because of bending at the anchorage due to the deflection of the girders under live load. Oscillation of the cables due to the various vibration mechanisms was an additional fatigue concern.

The two types of stay cables tested (HiAm SPWS-163 and NEW PWS-163) were both non-grouted parallel wire cables with button heads and a socket at both ends. Each cable had 163 individually galvanized wires with a diameter of 0.28 in (7 mm) and a tensile strength of 240 ksi (1670 N/mm^2). The free space within the socket was filled with a compound (steel balls, zinc powder, and epoxy resin) for the HiAm SPWS-163 cable and with a zinc-copper alloy for the NEW PWS-163 cable. Both cable configurations were covered with a polyethylene pipe. The cables were pre-stressed to a tension force of 330 – 440 kip (1470 –

1962 kN). The bending fatigue tests were performed using a displacement-controlled ram, which cycled the cable at mid-span (Figure 1-12).

Wiring breaking was monitored with accelerometers at both of the fixed ends of the cable and along the free length. The stresses were measured with strain gauges at various locations around the anchor head.

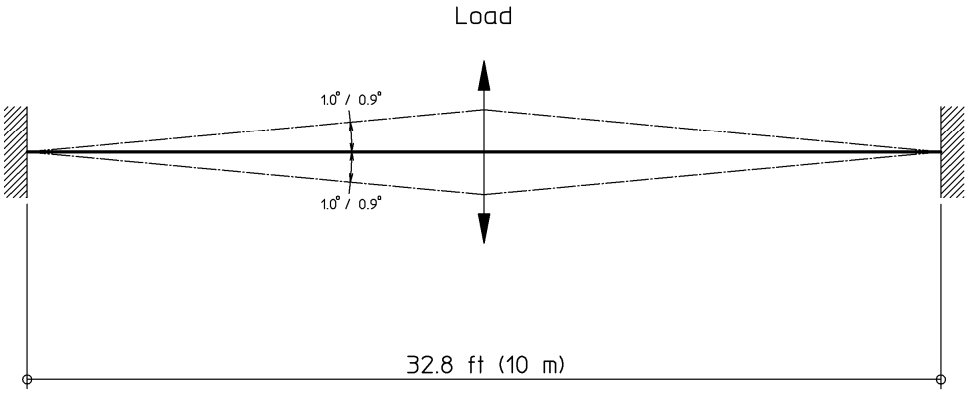

Figure 1-12: Japanese Bending Fatigue Test Steup

The estimated bending stresses at the end of the socket were ±29.0 ksi (±200 N/mm^2) for the NEW PWS-163 and ±30.4 ksi (±210 N/mm^2) for the HiAm SPWS-163 (Table 1-7).

Table 1-7: Test Results of Japanese Fatigue Tests

Stay Cable Type	**Bending stress at socket**	**α**
HiAm SPWS-163	±30.4 ksi (±210 N/mm^2)	±1.0°
NEW PWS-163	±29.0 ksi (±200 N/mm^2)	±0.9°

No fatigue failures were detected on either cable after 10 million cycles with applied bending angles of ±1.0° and ±0.9° respectively. The authors stated that the measured stresses within the socket had large variations. Therefore, it was assumed that the cable did not behave as a single elastic body.

The overall conclusion was that the tested stay cables behaved very well in fatigue. Follow-up tests using an angle range of ±1.35° for each cable produced fatigue failures at 0.262 million cycles for the HiAm stay and 0.326 million cycles for the NEW stay.

1.5.3 Comparison with Fatigue Studies of Prestressing Strand

Paulson (1983) summarized data from 341 published axial fatigue tests on single seven-wire strand and proposed a lower bound design curve.

In Figure 1.14 the mean value of Paulson's summary and his suggested design curve are compared with the axial fatigue requirement for stay cables and the Japanese bending fatigue tests on HiAm SPWS-163 and NEW PWS-163.

The results of the Japanese bending fatigue tests are far beyond the mean value of the axial data on seven-wire strand. The excellent performance might be due to the fact that the cable systems were not grouted parallel seven-wire cables but a HiAm and a NEW PWS anchorage with parallel wires respectively. However, even the fact that it is a different system leaves some doubts on the high performance. One of the key issues is the estimate of the stresses that occur during the test, generally a very difficult task.

The axial fatigue requirement for stay cables, 2 million cycles with a maximum of 2% wire breaks at a stress range of 23 ksi, does not seem to be very strict. One would assume that the strand in the free length and also in the transition region outside of the gripping area would fulfill the requirement with ease. However, as the earlier discussed test results show, it is generally difficult to achieve these requirements with grouted parallel seven-wire cable systems. It is even more surprising that most of the breaks do not occur in the gripping area but in the transition region and in the free length. The heavy corrosion that occurred

in a large number of tests may partially explain the failures. Ironically it appears that the grout, which should protect the strand from corrosion, might have something to do with the occurrence of corrosion that sometimes leads to very poor fatigue performance.

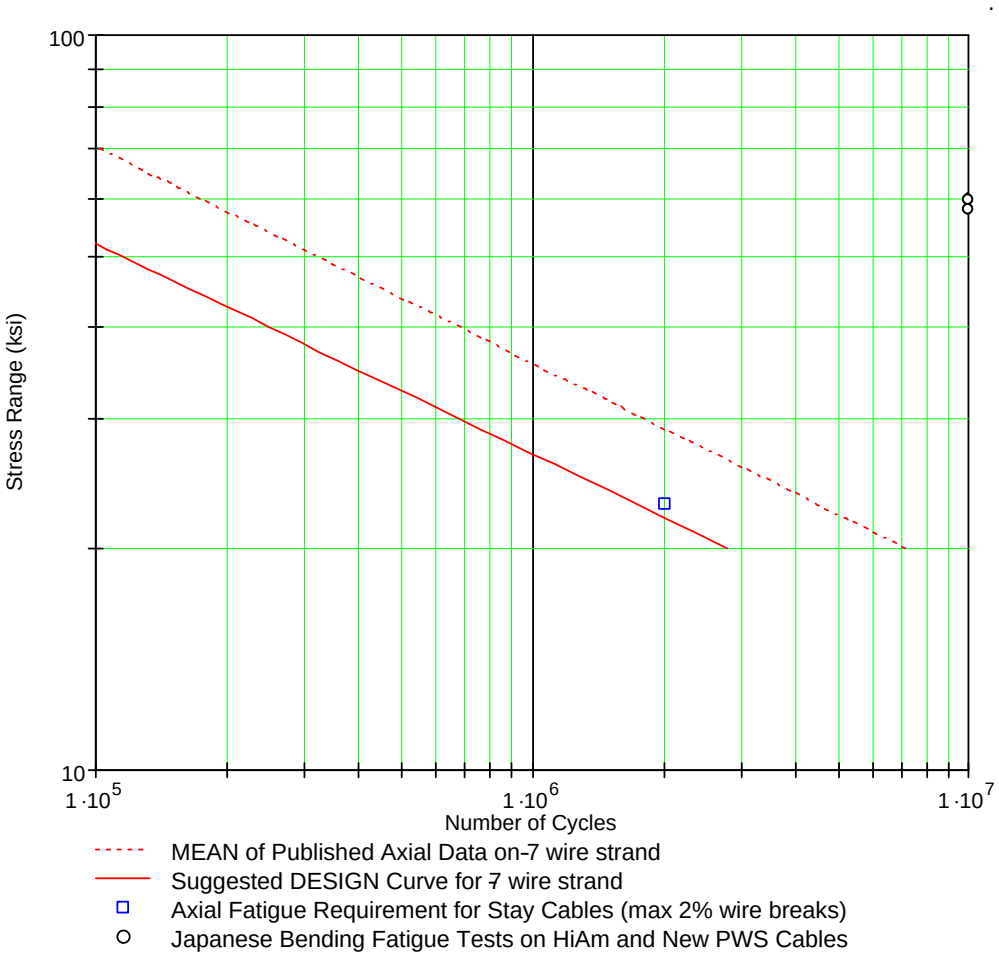

Figure 1-13: S-N Curves of Seven-Wire Strand by Paulson

CHAPTER 2

The Fred Hartman Bridge and its Stay Cables

2.1 INTRODUCTION

The Fred Hartman was opened to traffic on September 27th 1995. The main span of 1250 ft (381 m) crosses the Houston shipping channel between Baytown (TX) and La Port (TX). The bridge was necessary because the existing tunnel was overburdened and also because of plans to deepen the channel. The daily capacity is 200,000 vehicles, which is almost ten times higher than that of the old tunnel. Because of its aesthetically pleasing appearance, the Fred Hartman Bridge has become a landmark for the entire region (Figure 2-1).

Figure 2-1: Fred Hartman Bridge at Night

One of the most remarkable aspects of the Fred Hartman Bridge is its extreme width of 160 ft (49 m). The bridge is essentially made out of two independent decks, each 78 ft (24 m) wide. Both decks accommodate four lanes of traffic and two emergency lanes (Figure 2-2). The Fred Hartman Bridge is one of the largest cable-stayed bridges in the world in terms of overall deck area, due to its large width.

Figure 2-2: Bridge Deck seen from the Tower

The twin decks are carried by a total of 192 cables which radiate in a fan shape arrangement from the four diamond-shaped concrete towers. The towers are 436 ft (133 m) high and are joined at deck level to act as a truss under lateral load. The deck consists of steel plate girders with a large number of transverse floor beams and a precast concrete slab (Figure 2-3).

Figure 2-3: Bridge seen from Underneath

2.2 SUMMARY OF FRED HARTMAN BRIDGE

- Total length: 2,475 ft (754 m)
- Main span: 1250 ft (381 m)
- Eight-lane composite deck - 2 x 78 ft (24 m)
- Building time: 9 years from 1986 until 1995
- Opened to the traffic on September 27th 1995
- Replaced the Baytown-La Porte tunnel
- Capacity: 200,000 vehicles per day (Baytown tunnel: 25,000 per day)
- Cost: 100 million US Dollars
- Double diamond towers as tall as a 45-story building - 436 ft (133 m)
- Fan-type arrangement of the stay cables
- 192 cables, the longest stretching 650 ft (198 m)
- Over 618 miles (995 km) of cable strand
- More than 40,000,000 pounds (18,145 t) of steel
- More than 3,000,000 ft^3 (84,950 m^3) of concrete

Reference: National Web Window (2001)

2.3 CABLE AND ANCHORAGE DESIGN

Each of the four planes of cables, radiating from the towers (Figure 2-4), is attached to the outside of a steel plate girder at the deck level (Figure 2-5).

Figure 2-4: Cable Anchorage Tower

Figure 2-5: Cable Anchorage Deck

The cables are parallel-strand cables, which is one of the simplest cable systems available. The system consists of a bundle of parallel seven-wire 0.6-in (15-mm) strands that is surrounded by a polyethylene (PE) pipe. The remaining space between the individual strands and the PE pipe is grouted after the stressing of the strands. The PE pipe and the grout serve as corrosion protection for the steel strands. A special element is a helical spacer wire which ensures that there is always a minimum layer of grout between the PE pipe and the strand. Figure 2-6 shows the cross section of a stay with 19 strands along the free length. The PE pipe is further wrapped with yellow Tedler tape to increase the UV protection of the already UV resistant PE pipe.

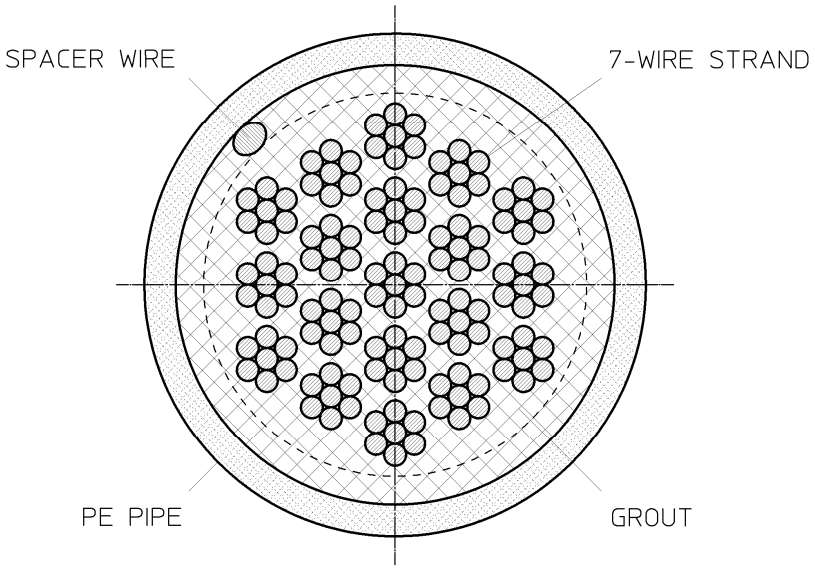

Figure 2-6: Cross Section Parallel-Strand Cable

The anchorages for the cables of the Fred Hartman Bridge are a VSL System. In the anchorage region, the strands, which are parallel in the free length, spread out to be anchored by a wedge system in the anchor head and then into a

load distribution plate which is attached to the steel plate girder. Figure 2-7 and Figure 2-8 show the components of anchorage at deck level.

The function of the tension ring is to resist the perpendicular force component, which results from the spreading of the strands. The two key elements of the anchorage region are the anchor head and the tension ring. The entire anchorage region is also covered with a PE pipe and also grouted after the stressing.

At deck level, an anchorage box and a steel guide pipe further cover the transition region. The steel guide pipe also incorporates a neoprene damper. At tower level, the transition region is only partly covered by a steel guide pipe which also incorporates a neoprene damper as shown in Figure 2-9 and Figure 2-10. One other difference between the two ends is the shim plates at the tower end, which is used during the prestressing of the stay cable which is done from the tower end. The shim plates can be seen as an extension of the load distribution plate and do not influence the bending of the stay cable anchorage since the shims are in contact with the transition pipe.

The four test specimens are essentially identical to the smallest cable diameters of the Fred Hartman Bridge. The only difference is that the length of the specimens is much shorter as further explained in Chapter 3.

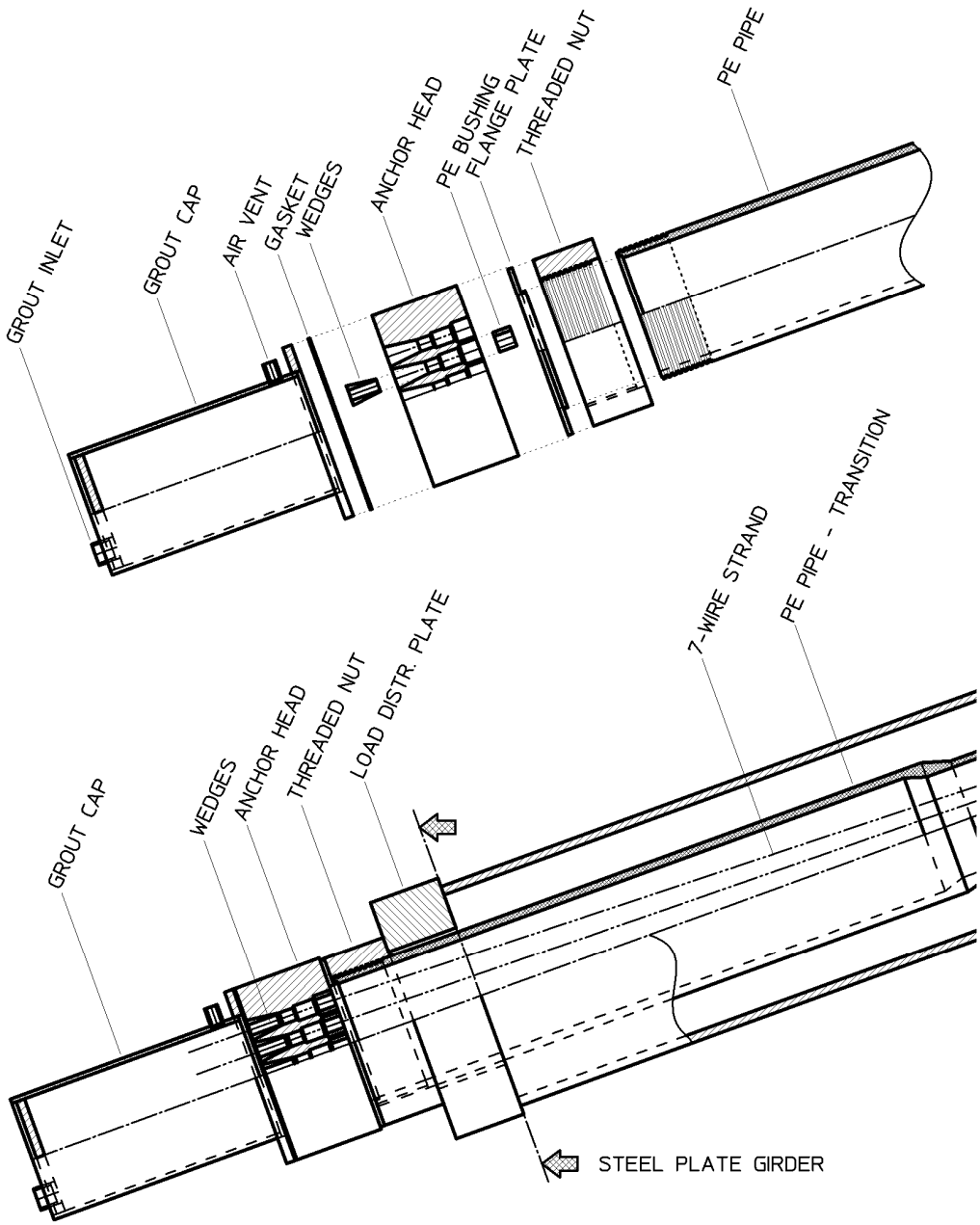

Figure 2-7: Deck Anchorage (I)

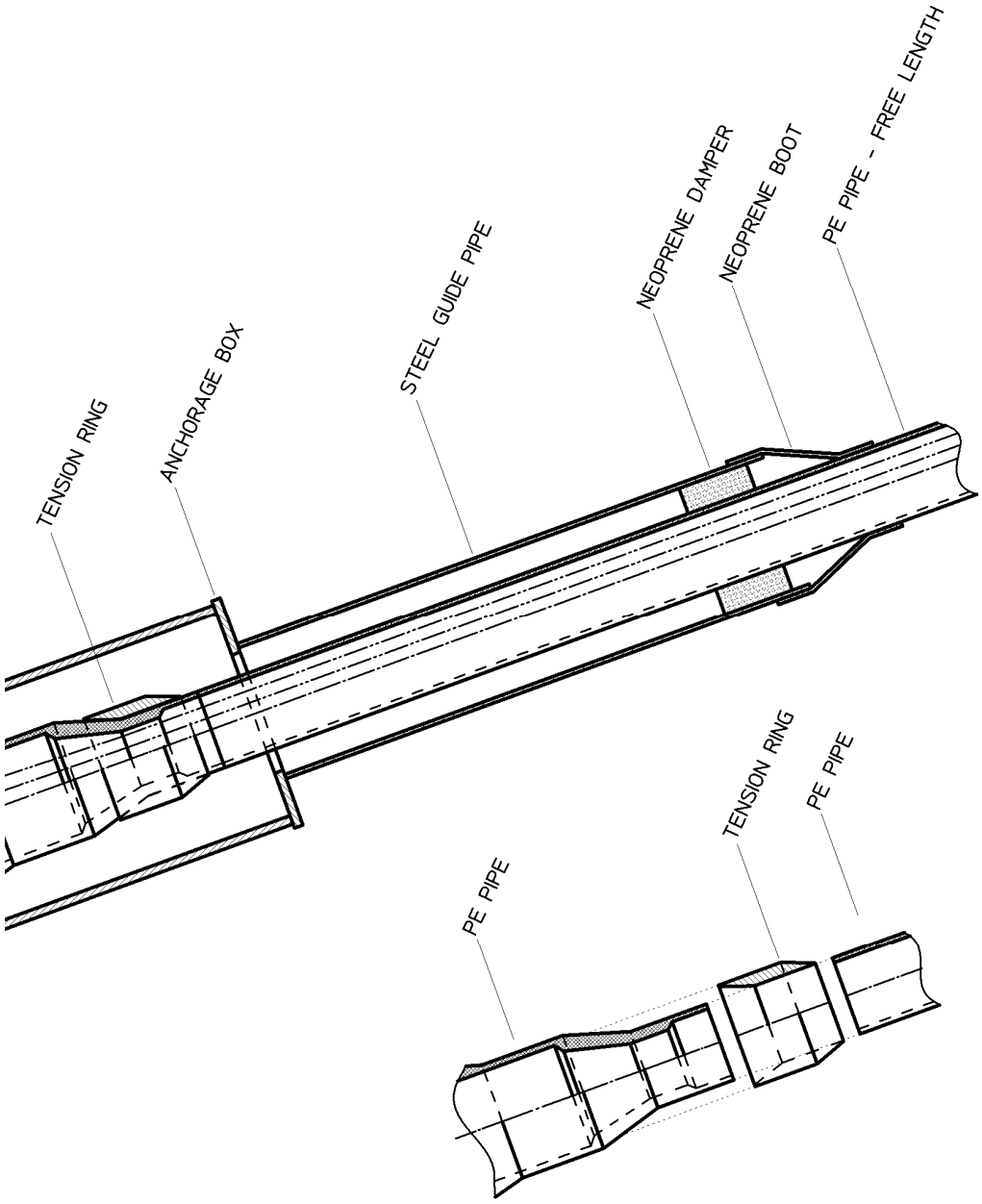

Figure 2-8: Deck Anchorage (II)

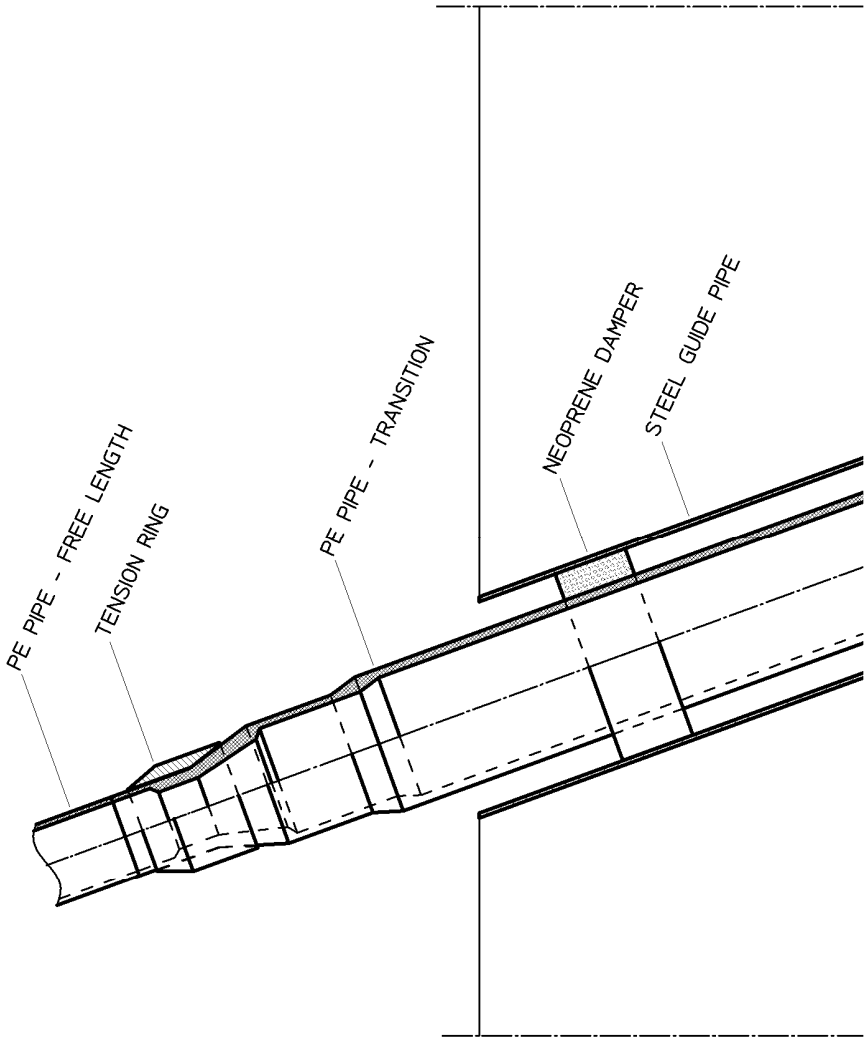

Figure 2-9: Anchorage Design Tower (I)

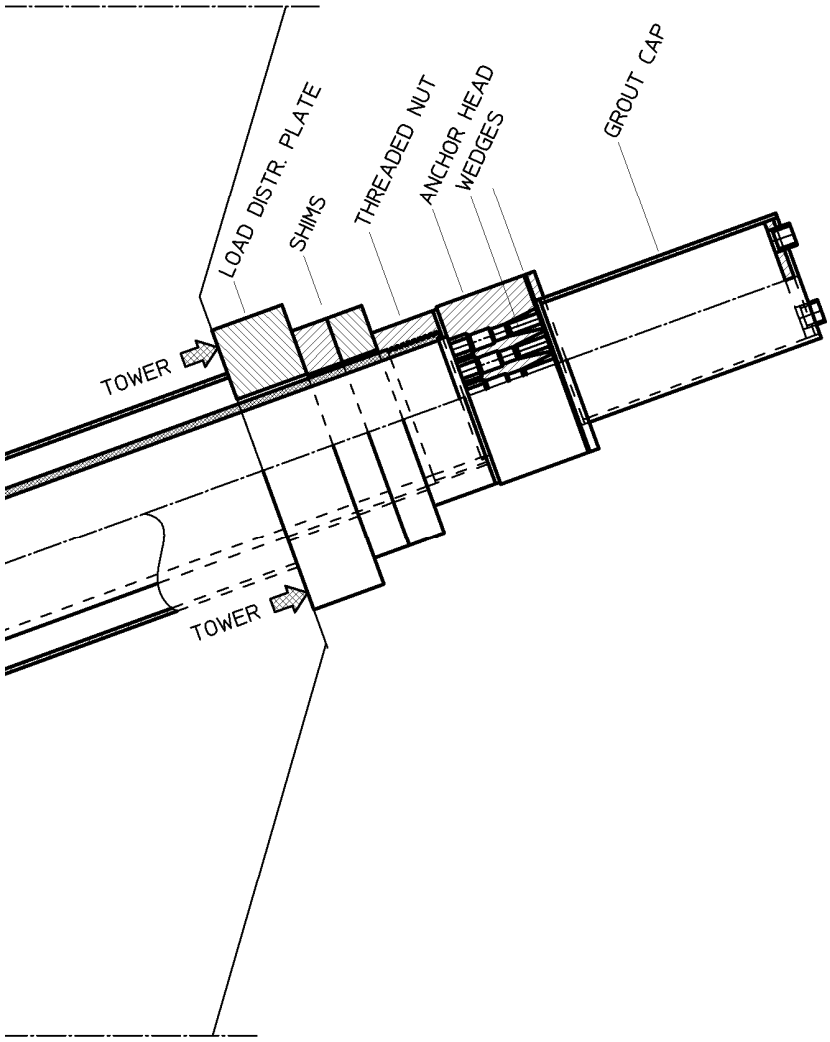

Figure 2-10: Tower Anchorage (II)

CHAPTER 3
Test Setup and Specimen Assembly

This chapter discusses how the dimensions of the stay cable specimen were determined. The details of the test setup used for the fatigue tests and the assembly of the stay cable specimen are also presented in this chapter.

3.1 INTRODUCTION

Preliminary finite element models (FEM) of stay cables during a vibration event showed that the areas with the highest curvatures, and therefore with the highest bending stresses, are expected to be in the anchorage region (Dowd 2001). Based on this information, the main focus of the full-scale bending fatigue test was on the behavior of the stay cable in the anchorage region.

To limit the size of the test setup, the cable diameter and the number of strands of the test specimen were chosen to be the same as the smallest cable on the Fred Hartman Bridge – a cable composed of 19 strands. It should be noted again that the design of the stay cables of the Fred Hartman Bridge was changed during construction because of axial fatigue concerns and an extra strand was added to all cables. Anchorage drawings that included the extra strand were unfortunately not available, and therefore the original design with the 19 strands was chosen as the basis for the stay cable test.

Each test specimen consists principally of the same elements as the actual stay cables of the Fred Hartman Bridge. The main difference is that the steel guide pipe with the neoprene damper is not used in the fatigue test. One hundred-one of the total of 192 guide pipes were broken on the Fred Hartman Bridge, and

consequently cable vibration occurred without the restraint of the guide pipe. In addition, it has been observed that even strengthened and stiffened guide pipes do not prevent the stay cable from vibrating. However, they might reduce the bending moment at the anchorage.

The terminology of “deck anchorage” and “tower anchorage” is also used for the test specimens although the specimen is tested horizontally. The tower anchorage is the end of the test specimen that is at the top during the inclined grouting procedure.

Further FEM were performed so as to find the ratios of the curvature, steel stress, and grout stress between the anchorage and the tension ring on a laboratory specimen and to match those values with those on an actual stay cable (Dowd 2001). The FEM showed that a point load applied at mid span of a 32-ft (9.7-m) specimen, with the tension ring at 40 in. (1 m) from the anchorage, predicts a good correlation. The preliminary geometry is shown in Figure 3-1. Note that the design was completed without an experimental verification of the model.

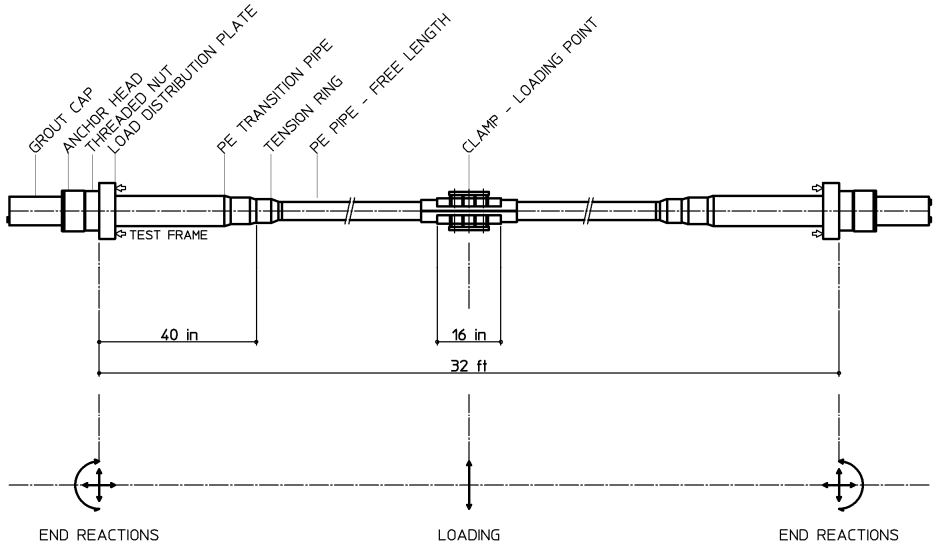

Figure 3-1: Preliminary System of the Test Setup

The specimen does not allow the studying of the bending fatigue behavior of the stay cable in the free length. Only the anchorage region is modeled in the fatigue test. Figure 3-2 indicates that there might be points of concern along the length of the stay, as for example the points of maximum deflection, which are not reproduced in the fatigue test.

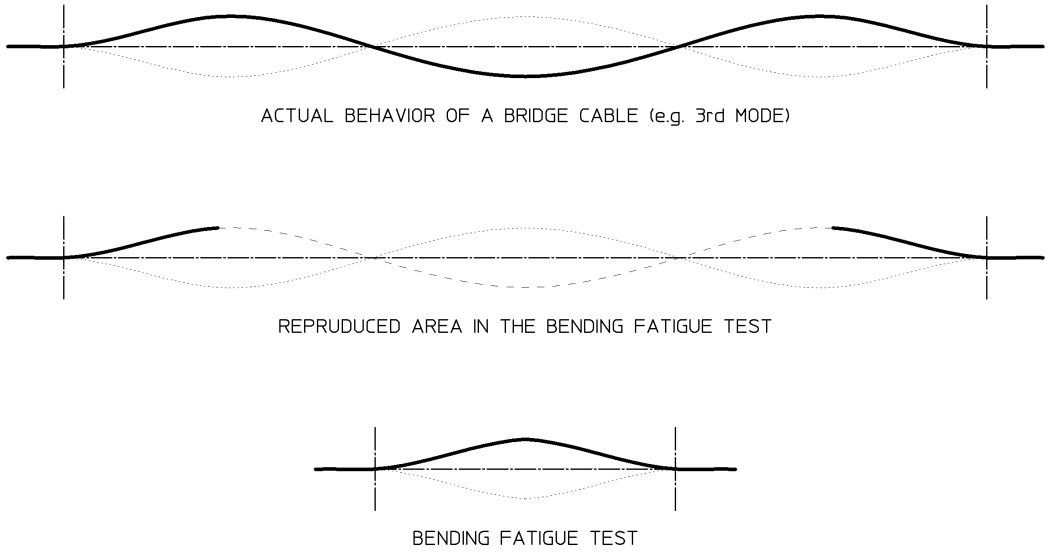

Figure 3-2: Actual and Reproduced Behavior

The estimated forces for the design of the test setup from a conservative preliminary FEM of a test specimen with a length of 32 ft (9.75 m) with amplitude at mid span of +/- 1.6 in. (40 mm) are presented in Table 3-1. It should be noted at this point that the ram force required during the actual tests was only +/- 7.6 kip (33.8 kN), which would result in a shear force of +/- 3.8 kips (16.9 kN) at the anchorage as shown in Table 3-2 and Table 3-3.

This observation indicates that the FEM appears to have been too stiff, which leaves open the question on the accuracy of the models of the actual bridge cables and the intended match in curvature. This point is discussed further in Chapter 5.

Table 3-1: Estimated Force and Displacement - FEM

Prestressing (static)	445	kip	1980	kN
Test Ram Amplitude	+/- 1.6	in.	+/- 40	mm
Test Ram Force (cyclic)	+/- 16	kip	+/- 71.2	kN
Anchorage Moment (cyclic)	+/- 15	kip in	+/- 20	kNm
Shear (cyclic)	+/- 8	kip	+/- 35.6	kN
Axial (cyclic)	+/- 6	kip	+/- 26.7	kN

Table 3-2: Measured Force and Displacement - Fatigue Test

Prestressing (static)	445	kip	1980	kN
Test Ram Amplitude	+/- 1.6	in.	+/- 40	mm
Test Ram Force (cyclic)	+/- 7.6	kip	+/- 32.9	kN
Anchorage Moment (cyclic)	N/A	kip-in	N/A	kNm
Shear (cyclic)	+/- 3.8	kip	+/- 16.9	kN
Axial (cyclic)	N/A	kip	N/A	kN

Table 3-3: Difference between FEM and Measured Force and Displacement

Prestressing (static)	0	kip	0	kN
Test Ram Amplitude	0	in.	0	mm
Test Ram Force (cyclic)	+/- 7.4	kip	+/- 37.4	kN
Anchorage Moment (cyclic)	N/A	kip-in	N/A	kNm
Shear (cyclic)	+/- 4.2	kip	+/- 18.7	kN
Axial (cyclic)	N/A	kip	N/A	kN

3.2 TESTING APPARATUS

A stressing frame consisting of two longitudinal wide flange columns and built up crossbeams at both ends was used to react the initial stressing force and the forces from the fatigue test. A portal frame is used at mid span to mount the test ram. The test specimen is clamped at mid span with a steel clamp that is bolted to the ram.

Figure 3-3: Testing Apparatus

3.2.1 Reaction Frame

Two longitudinal W14x90 columns serve mainly as axial compression members. The axial forces result mainly from the prestressing of the stay cable. A secondary axial component results from the change in axial load in the cable during the fatigue test. The longitudinal wide flange columns also provide the bending stiffness, which is necessary to react the end moments occurring in the fatigue test.

The built up crossbeams at both ends consist of two W18x97 beams with welded stiffeners and a load distribution plate with an opening for the stay cable. The load distribution plate is in direct contact with the threaded nut or the shim plates of the stay cable and directs the forces from the stay cable into the test frame. The vertical shear forces are anchored into the lab floor using a T-section with anchor bolts as shown in Figure 3-4 and Figure 3-5.

The forces given in Table 3-1 were used as a basis for the design along with a safety factor of 2.0 to size the members of the test frame. All members of the test frame are of Grade 50 steel. Because of the cyclic loading that is applied at mid-span, the frame was further designed considering fatigue and dynamic behavior. The fatigue stress range in the frame during the actual bending fatigue test under the given loads from Table 3-1 does not exceed 5 ksi (20 N/mm^2). The lowest natural frequency for the T-section is 4 Hz and 7 Hz for the longitudinal columns, which are both higher than the loading rate of 1 - 2 Hz.

The geometry of the reaction frame provides space for specimens with a length of 32 ft 7 3/8 in. (10.58 m), which is slightly larger than the 32 ft (9.75 m) used in the FEM. As shown in Chapter 2, the anchorage at the tower end of the stay cable has two shim plates between the treaded nut and the load distribution plate. The shim plates can be considered as an extension of the load distribution plate since they are not in contact with the stay cable but only with the threaded nut. To replicate the actual cables of the Fred Hartman Bridge, the shim plates were used in the test which adds an extra 4 in. (100 mm) at the tower side. The total length of the stay cable specimen is therefore 32 ft 11 3/8 in. (10.68 m). Further comments on the geometry can be found in Section 3.3.

The reaction frame was also designed to be movable with an installed and pre-tensioned specimen. This is necessary because the grouting of the specimen is in an inclined position, whereas the bending fatigue test is in a horizontal position.

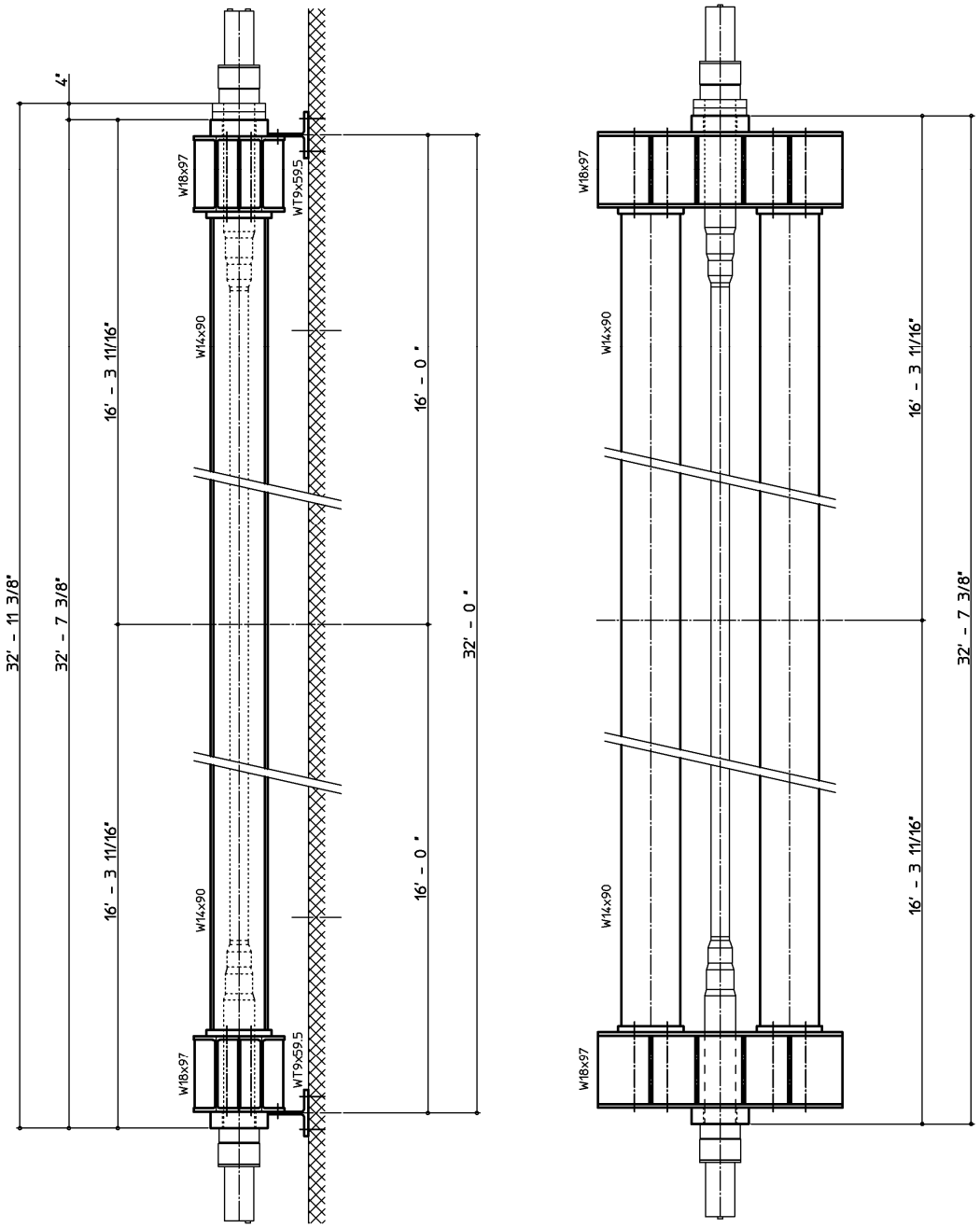

Figure 3-4: Geometry - Reaction Frame

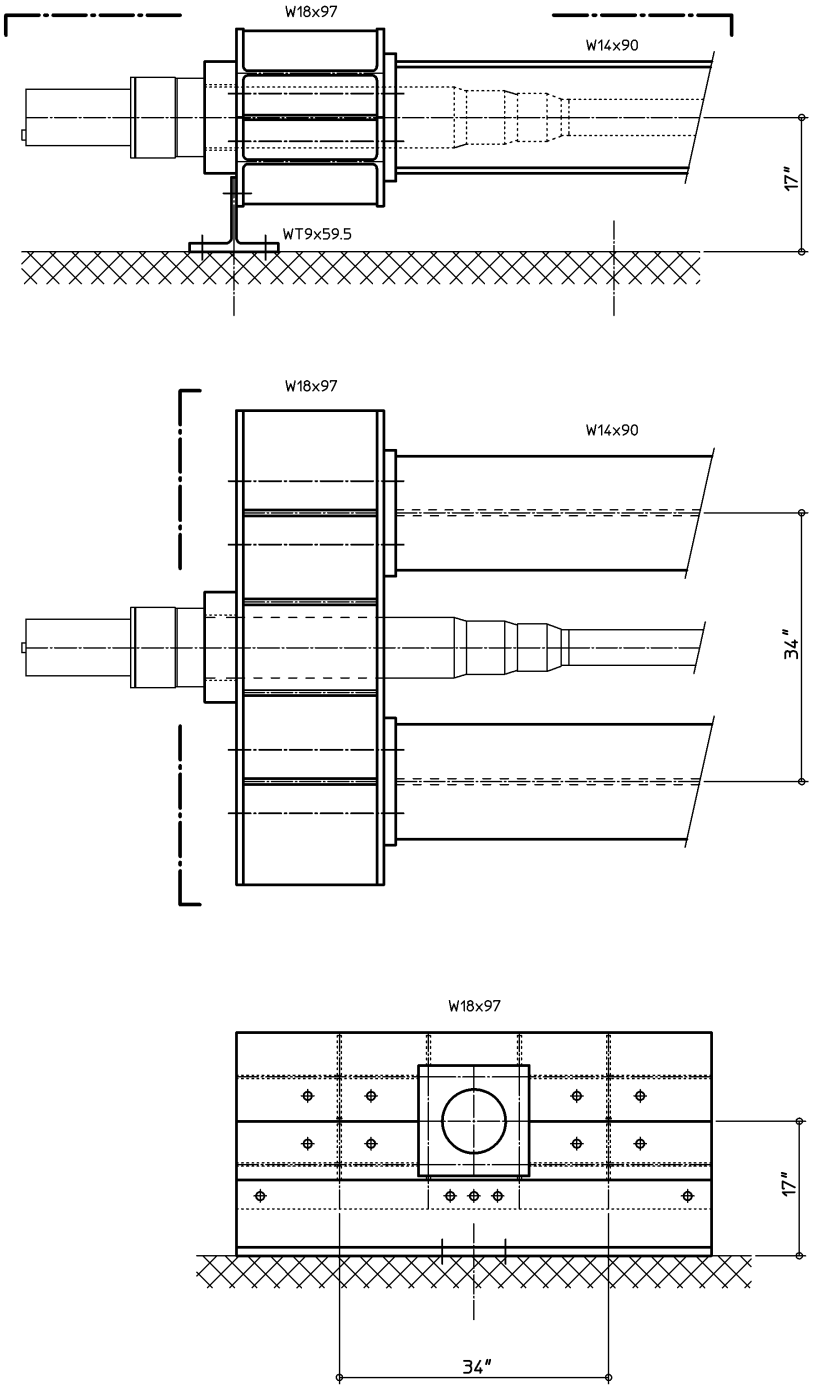

Figure 3-5: Geometry - Cross Beam

3.2.2 Portal Frame

The portal frame at mid-span reacts the test ram at mid-span. The frame consists of two W12x58 columns and two W24x84 cross beams (Figure 3-6). The test ram is attached to the cross beams with four 1 in. (25 mm) rods.

Figure 3-6: Portal Frame

3.2.3 Clamp – Load Point

The clamping region was designed to minimize stresses in the stay and to keep the length of this disturbance region to a minimum. The solution was to cushion the stay cable in the clamping region with an extra layer of polyethylene over a length of 22 in. (560 mm) and to grip the cushioned stay cable with a steel clamp over a length of 16 in. (405 mm). The steel clamp consists of a top and bottom steel shell with stiffeners and connections details for four 1-in. (25-mm) rods to connect the test ram as shown in Figure 3-7 and Figure 3-8.

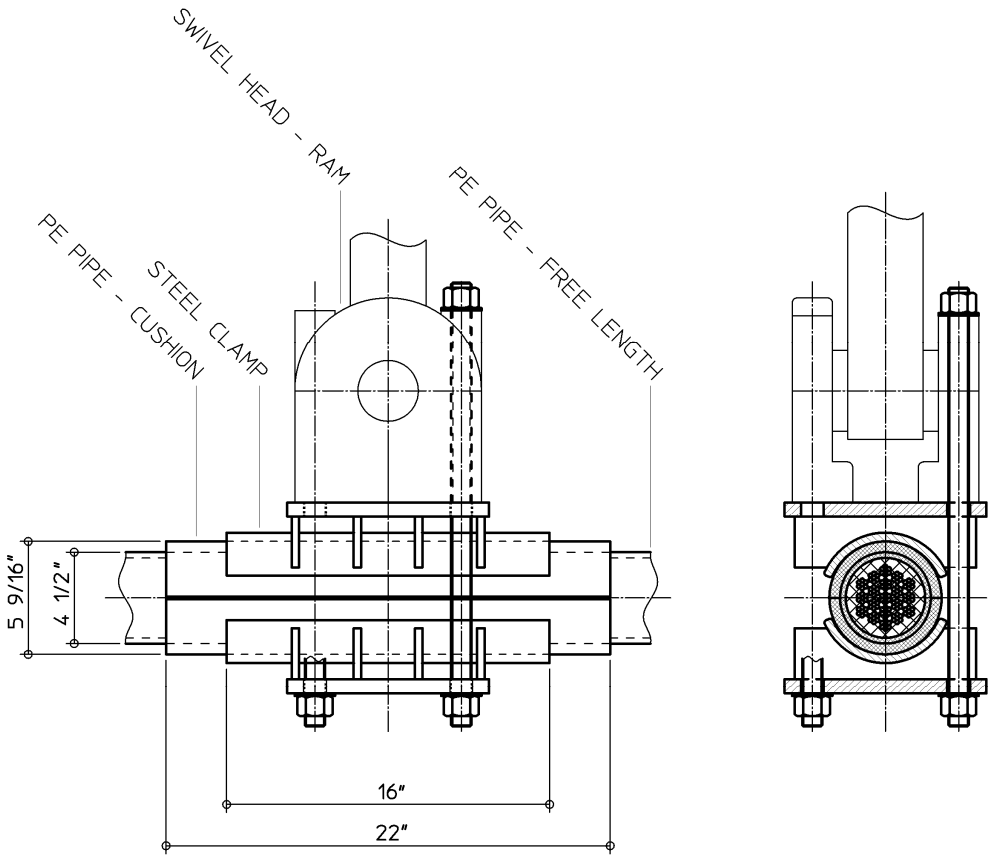

Figure 3-7: Clamp – Load Point

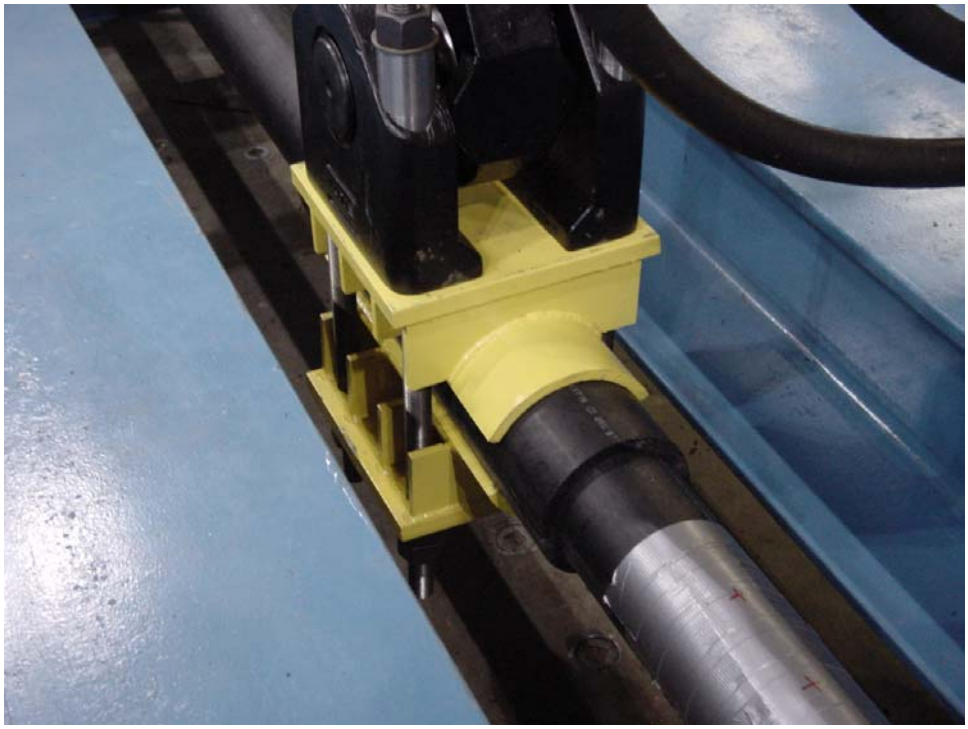

Figure 3-8: Assembled Clamp

For the second specimen, the design of the clamp was slightly modified, in an attempt to reduce the stresses in the stay at the ends of the clamp. The inside of the PE cushioning pipe was tapered over a length of 1 in. (25 mm) to provide a smoother transition between the stay cable and the clamping region.

The clamp performed reasonably well in the fatigue test, as discussed in Chapter 4. Possible modifications for the clamp for further tests would be to taper the outside of the PE cushioning pipe instead of the inside. Furthermore, the same idea could be used for the steel shells. These measures would reduce the stiffness in the taped regions to allow a smooth increase in stiffness from the stay cable to the PE cushioning pipe and to the steel shells.

3.2.4 Hydraulics

The hydraulic setup used for the fatigue test is a closed loop system, shown in Figure 3-9, consisting of two hydraulic pumps, an MTS line conditioner, a linear MTS hydraulic actuator (Figure 3-6), and an MTS Controller.

The two hydraulic pumps have a total capacity of 75 gallons per minute (256 lt/min). The MTS actuator is fatigue rated and has a stroke of +/- 5 in. (+/- 127 mm) and a rated force capacity of 55 kips (244.7 kN). The actuator is further equipped with a coaxially mounted LVDT displacement transducer and an axial load cell. The two servo valves on the test ram have a total capacity of 30 gpm.

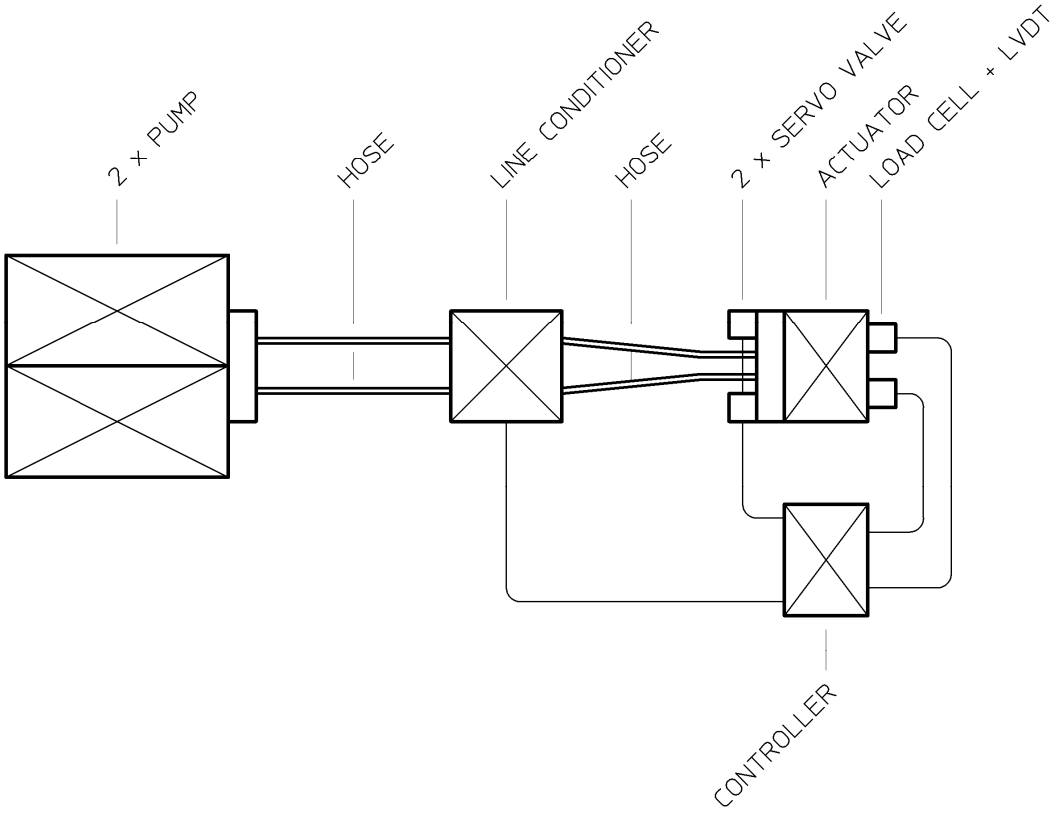

Figure 3-9: Hydraulic Scheme

3.3 STAY CABLE SPECIMEN

The specimen consists of 19 seven-wire 0.6-in. (15-mm) strands and has a length of 32 ft 11 3/8 in. (10.68 m) from the threaded nut at the deck anchorage to the threaded nut at the tower anchorage.

The design of the test specimen is basically identical to the stay cables of the Fred Hartman Bridge. Figure 3-10 shows the elements of the anchorage and how they are assembled, Figure 3-11 shows the specimen geometry, and Figure 3-12 the cross sections of the cable. As mentioned earlier and shown in Figure 3-11, the specimen is 4 in. longer on the tower side because of the shim plates. This difference in length would theoretically result in a slightly lower bending moment at the tower end. Beside this length difference, the specimen is symmetric about the loading point.

VSL International, the cable supplier for the Fred Hartman Bridge, fabricated the individual elements of the anchorages. The fabrication was based on the latest set of drawings of the stays of the Fred Hartman Bridge that were available. As mentioned earlier, the as-built stay cables have one extra strand because of axial fatigue concerns. The PE pipe in the free length is industrial high-density PE pipe with an outside diameter of 4.5 in. (115 mm) and an inside diameter of 3 15/16 in. (100 mm). The strand is ASTM A416 seven-wire 0.6 in. (15 mm). It was delivered in spool of 8500 ft (2,600 m). Table 3-4 and Table 3-5 present the ATSM specification values and the actual mill certificate values. All values fulfill the ASTM requirements.

Table 3-4: Mechanical Properties - ASTM

Grade	**270 K**	
Nominal Diameter	0.6 in	15.24 mm
Strand Tolerance	0.6102 / 0.5941 in	15.50 / 15.09 mm
Modulus of Elasticity	27500 ksi	190,000 N/mm^2
Min. Breaking Strength	58.6 kip	261 kN
Min. Yield Strength	52.74 kip	235 kN
Nominal Area	0.2170 in^2	140.00 mm^2
Nominal Weight	740 lbs/1000 ft	1,102 kg/1000m

Table 3-5: Mechanical Properties - Mill Certificate

Grade	**270 K**	
Modulus of Elasticity	28000 ksi	192890 N/mm^2
Min. Breaking Strength	58.992 kip	262.4
Min. Yield Strength	54.363 kip	241.81 kN
Nominal Area	0.2185 in^2	140.99 mm^2
Nominal Weight	740 lbs/1000 ft	1,102 kg/1000m

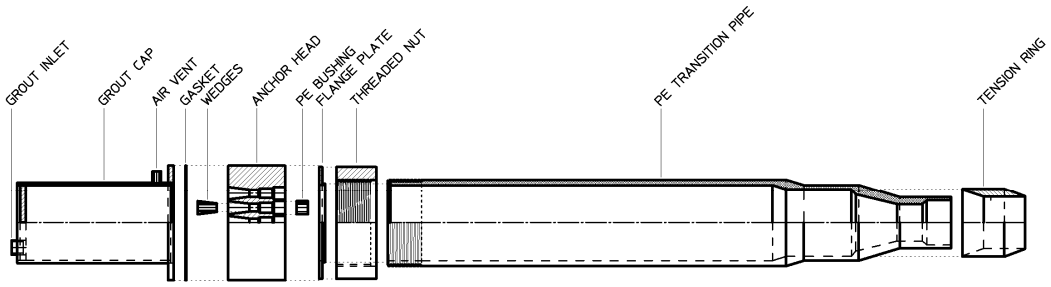

EXPLODED VIEW

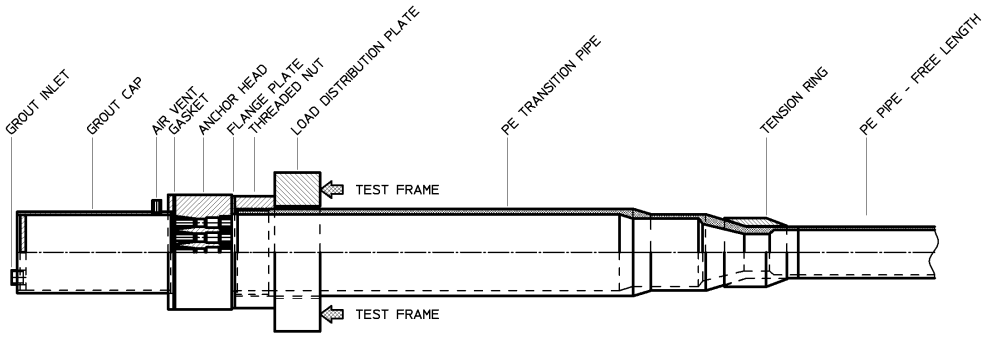

DECK ANCHORAGE

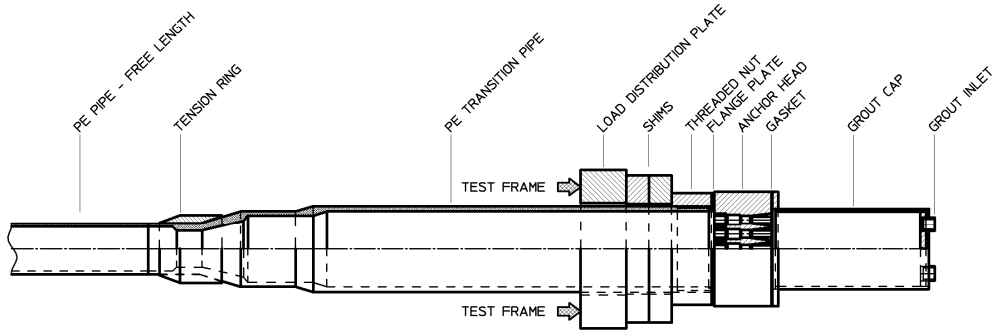

TOWER ANCHORAGE

Figure 3-10: Anchorage Elements of the Stay Cable Specimen

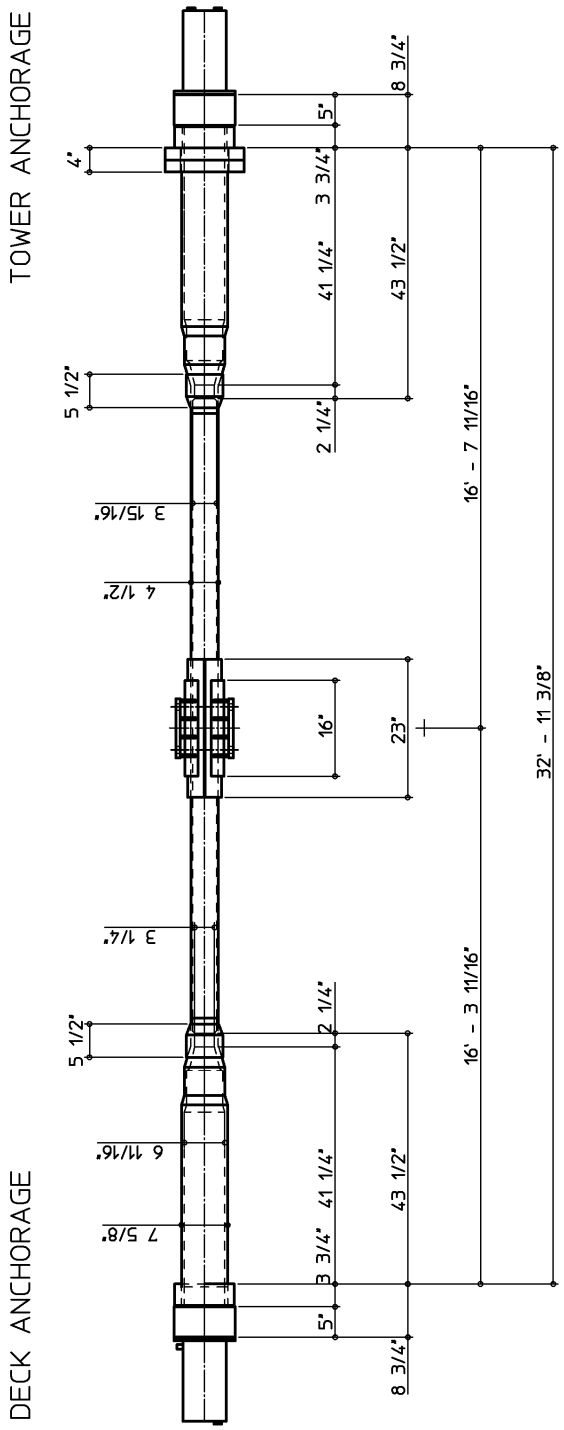
TOWER ANCHORAGE
DECK ANCHORAGE
4"
5 1/2"
3 15/16"
4 1/2"
3 1/4"
5 1/2"
6 11/16"
7 5/8"
5"
3 3/4"
41 1/4"
2 1/4"
43 1/2"
8 3/4"
16"
23"
16' - 7 11/16"
16' - 3 11/16"
32' - 11 3/8"

Figure 3-11: Geometry of the Stay Cable Specimen

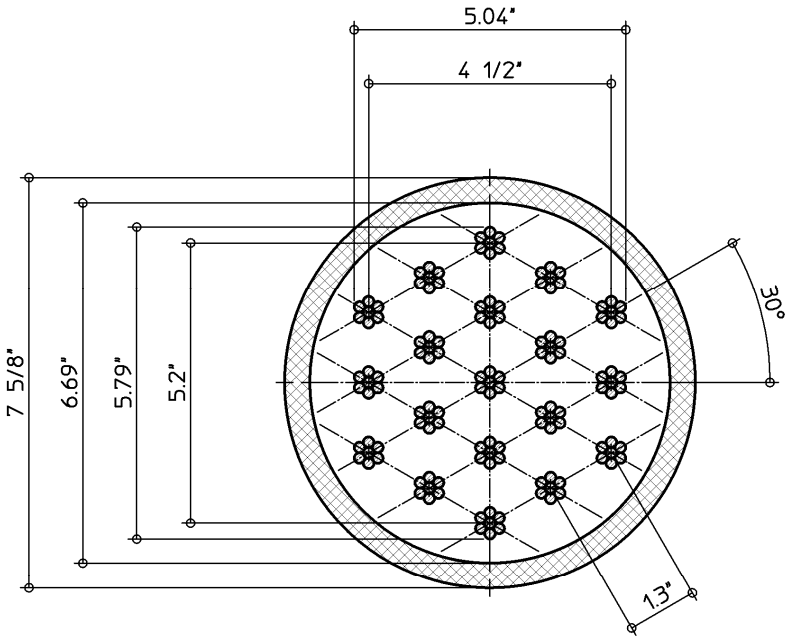

AT THE ANCHOR HEAD

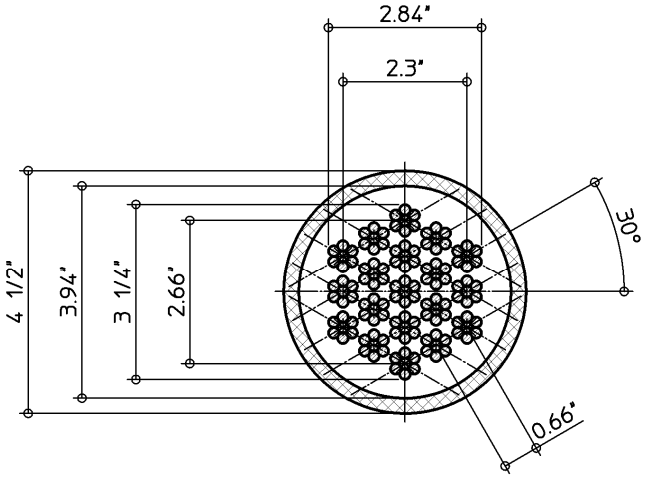

IN THE FREE LENGTH

Figure 3-12: Cross Section of the Stay Cable Specimen

3.3.1 General Assembly of a Stay Cable Test Specimen

The assembly of the stay cable specimen into the reaction frame and the grouting is presented step by step. Figure 3-20 and Figure 3-21, which can be found after step 9, are a schematic representation of the main steps of the assembly.

The assembly procedure consists of the cable installation starting at the tower end and working towards the deck end, the initial and final stressing from the tower end, and the grouting in an inclined position where the tower end is on top and the deck end on the bottom.

1. A total of 19 strands with a length of 48 ft (14.6 m) were cut from the strand spool (Figure 3-13). The final length required for the stay cable specimen was roughly 36 ft (11 m). The additional length was needed for the prestressing.

Figure 3-13: Cutting Strand

2. The entire tower anchorage consisting of the tension ring, PE transition pipe, shims, threaded nut, flange plate, and anchor head as shown in Figure 3-10, was installed and centered in the test frame.

3. The 19 strands were individually inserted into the corresponding opening in the anchor head (Figure 3-14) starting with the bottom strands. The strands were individually fed through the very congested tension ring region. This procedure ensured that the strands remained uncrossed in the transition region.

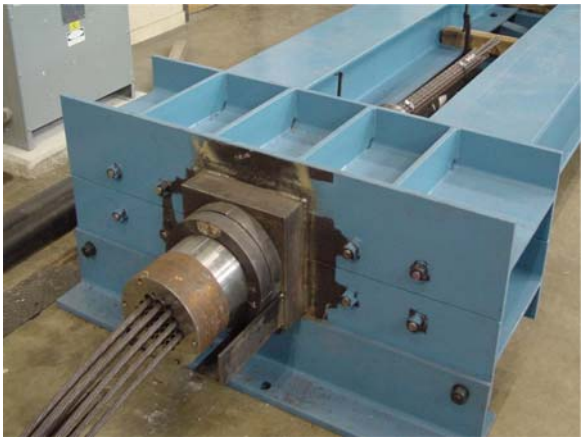

Figure 3-14: Strands Inserted through the Anchor Head

4. All 19 strands were pulled as a bundle from the tower side of the frame to the deck side and through the opening in the crossbeam (Figure 3-15). The pulling was done manually or with a forklift using a rope.

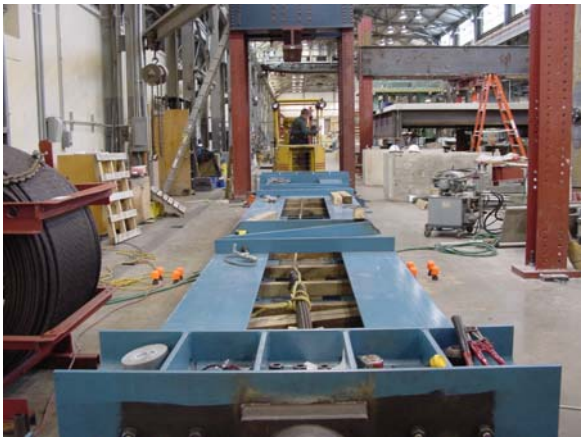

Figure 3-15: Strand Installation

5. The PE pipe (incl. the spacer wire) was inserted into the test frame from the deck side and slid over the bundle of the 19 strands (Figure 3-16).

Figure 3-16: PE Pipe Installation

The helical spacer wire was made of 0.25-in. (6-mm) steel wire. The wire was wound into a closely-spaced spiral with an inside diameter of 7.5 in. (190 mm) and stretched to its required outside diameter of roughly 4 in. (100 mm). The spiral was inserted into the PE pipe between the tension rings.

Figure 3-17: Helical Spacer Wire – Manufacturing and Inside the PE Pipe

6. The transition pipe with threaded nut and flange plate was inserted over the bundle of the 19 strands at the deck side.
7. The strands were installed in the deck anchor head in the same position as at the tower anchorage.

8. The wedges were installed into both anchor heads (Figure 3-18)

Figure 3-18: Installed wedges

The VSL wedge system consists of two halves that fit into the tapered opening in the anchor head (Figure 3-19).

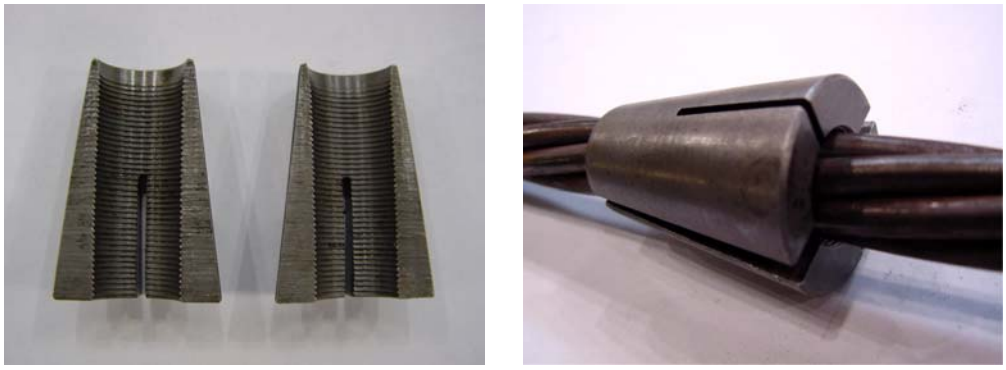

Figure 3-19: Wedges

9. The wedges at the deck side end were held in place by springs using a spring-loaded plate shown in Figure 3-26. This was done to ensure equal wedge seating on all the strands.

Deck End Tower End

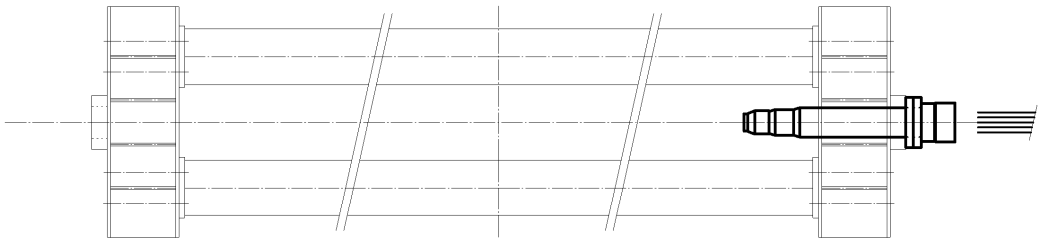

STEP 1 / 2

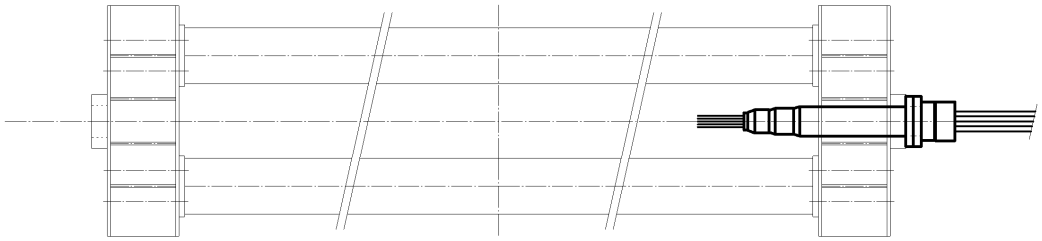

STEP 3

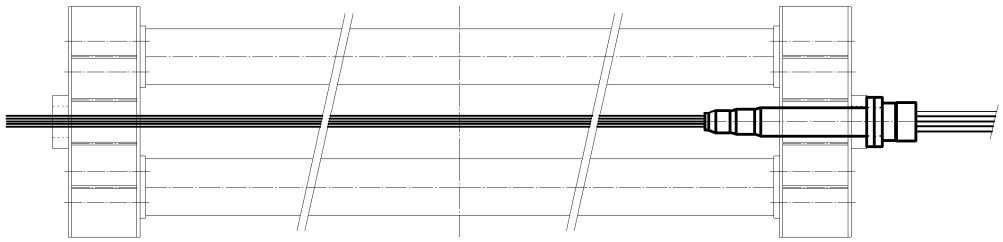

STEP 4

Figure 3-20: Stay Cable Specimen Installation (Steps 1 – 4)

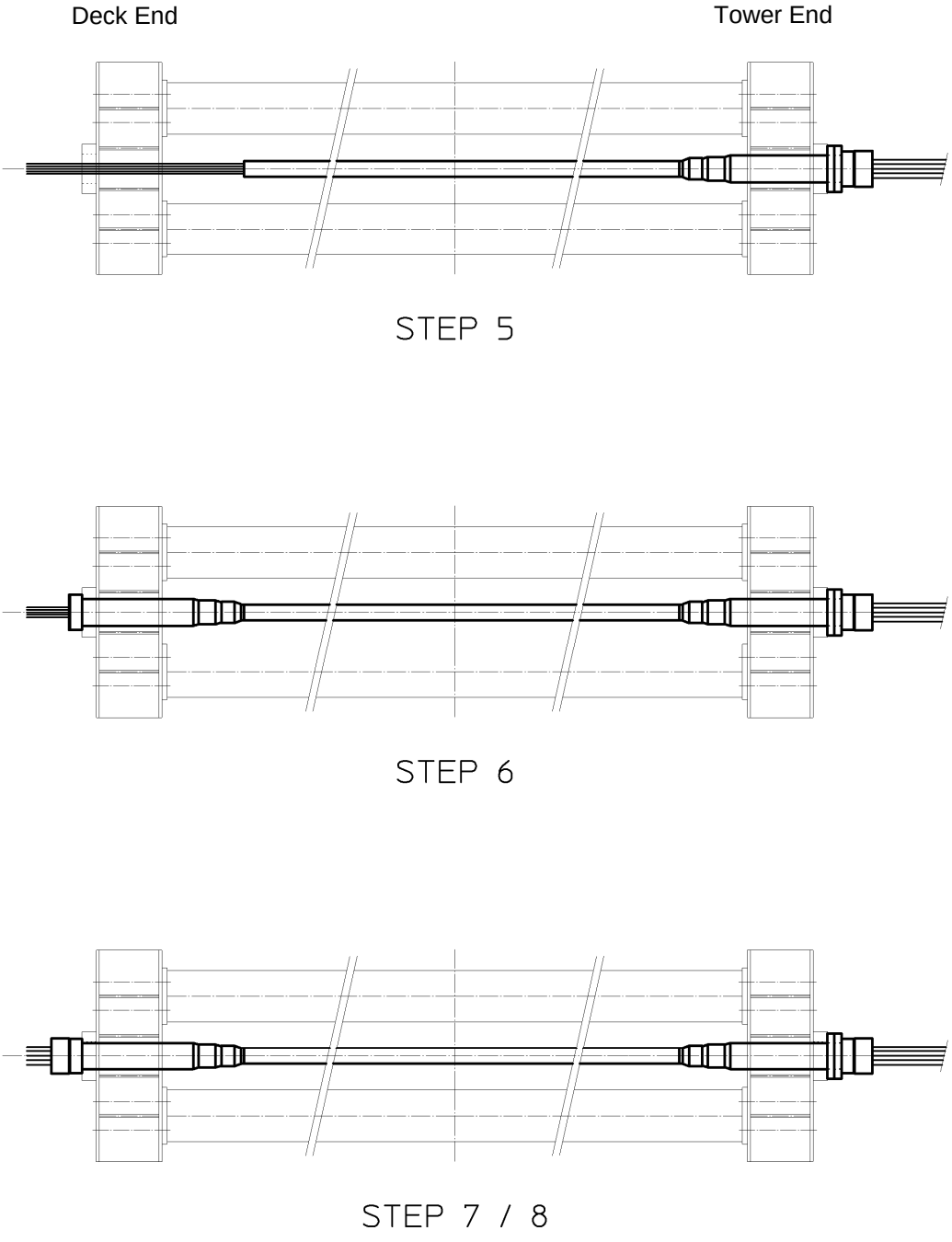

Figure 3-21: Stay Cable Specimen Installation (Steps 5 – 8)

10. Starting with the center strand and working to the outside, each individual strand was tensioned to an initial tension of roughly 1.5 kips using a mono-strand ram powered by an electrical pump (Figure 3-22). This procedure straightened the strands and seated the wedges.

Figure 3-22: Mono-Strand Ram Stressing

A specially fabricated tapered adapter was necessary to be able to react the ram against the very congested back face of the anchor head. The adapter also incorporated springs that applied a constant pressure to seat the wedges while the strand was initially stressed (Figure 3-23).

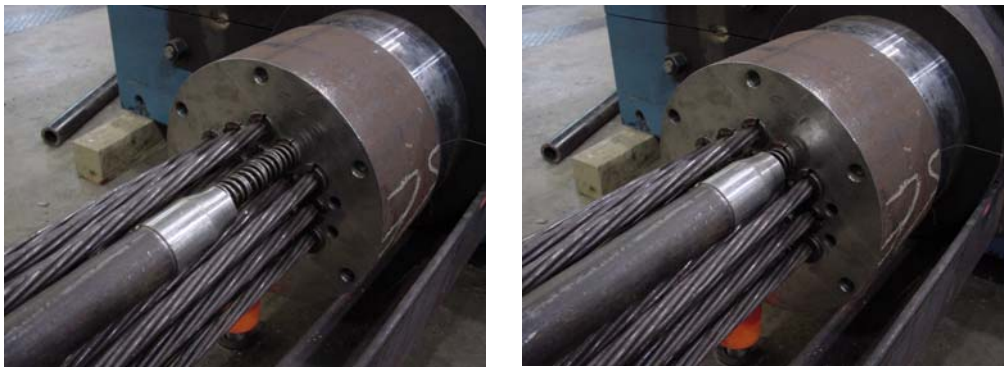

Figure 3-23: Spring Loaded Adapter for Mono Ram

11. All 19 strands were pulled together to prestress the stay cable specimen (Figure 3-24). The prestressing force in the cable was 445 kips (1,980 kN), which represents 40% of the guaranteed ultimate tension force (GUTS). The 40% value represents the dead load component in the actual bridge. The prestressing ram was installed between the tower end anchor head and an extra anchor head, which is used only for the stressing operation. The applied tension was controlled using a pressure gauge at the ram. The ram was powered using an electrical pump.

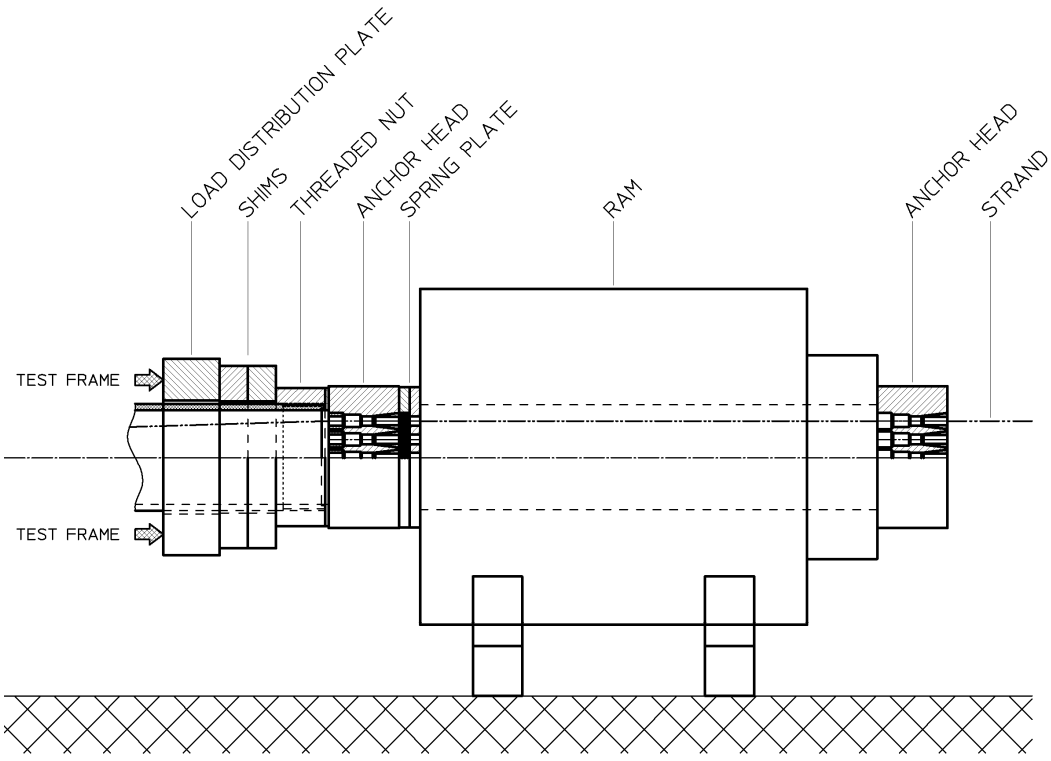

Figure 3-24: Setup for Stressing

The pressure on the ram was released after 50% of the tension force was applied and then retensioned. The specimen was then loaded to roughly 98% of the desired tension force before the pressure in the ram was released again

to roughly 50% of the maximum required pressure. This last step was performed 3 to 5 times until all wedge seating noises from the stay cable specimen disappeared. The mentioned noises appeared at a load level of 85% to 95% of the final tension force of 445 kip (1,980 kN). In the last step, the specimen was then brought up to its final tension force.

Figure 3-25: Final Stressing

A spring plate that incorporated 19 springs, which applies a constant pressure to the individual wedges, was used to seat the wedges at the stressing end (Figure 3-26). This ensured equal wedge seating and minimized the wedge seating loses in the stay cable specimen.

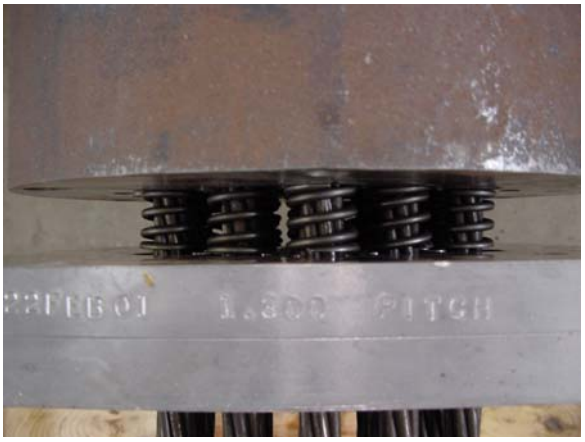

Figure 3-26: Spring Loaded Plate for Stressing

12. The PE transition pipe and the PE free length pipe were welded together using a commercially available plastic welder (Figure 3-27).

Figure 3-27: PE Welding

13. The reaction frame with the tensioned stay cable specimen was setup in an inclined position at an angle of roughly 30 degrees with the tower end at the top and the deck end at the bottom. A combined grout mixer and pump was used for grouting the stay cable (Figure 3-28).

Figure 3-28: Setup for Grouting

The grout consisted of Type I Portland cement and tap water. The water cement ratio was 0.42 and an anti-bleed admixture (Sikament 300 SC) with the recommended dosage of 2.2% was used for the second specimen. The components were first carefully mixed in the disc mixer before being released into the storage trough. The grout was pumped from the trough into the inlet of the grout cap at deck level. This procedure was performed until steady grout flow was observed in the transparent hose, which was connected to the grout cap at the tower end. The valve at the tower end was then closed and pumping was continued for a few more seconds to pressure the grout to ensure good grout filling and to reduce grout voids in the stay cable specimen. Note that this procedure does not necessarily represent a procedure used in the field. However, no specifications on grouting are available, which makes the grouting operation a somewhat uncertain and uncontrolled procedure. After the pump was shut off, the valve at the deck end was closed.

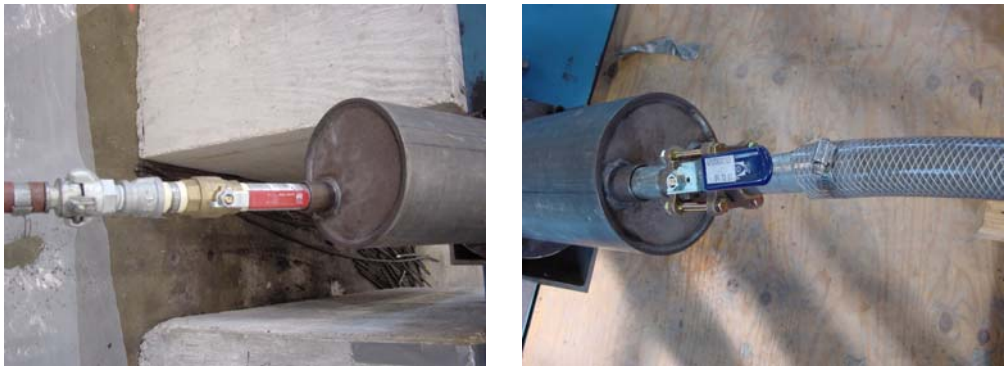

Figure 3-29: Grout Inlet and Outlet

The pumping pressure was monitored with a pressure gauge at the outlet of the pump. The dynamic pressure during pumping increased from 30 psi at the beginning to 60 psi at the end of the grouting. The corresponding static

pressures varied from 0 to 25 psi. The pump was shut off at a pressure level of 80 psi when the tower valve was closed during the pressurization of the stay.

3.3.2 Details of Specimen #1

The anchor head was orientated with the four grout inlets and outlets placed on the side of the anchor head as shown in Figure 3-30. This orientation of the anchor head might have caused a grout void at the tower end of the stay. However, there are no mechanical aids on the bridge anchorage that ensure correct placing of the anchor head nor is there a special note on the drawings. Furthermore, it was found that some of the larger stays on the Fred Hartman Bridge have grout outlets within the strand pattern. This means that there are always strands above the grout outlet, very similar to the configuration in test #1.

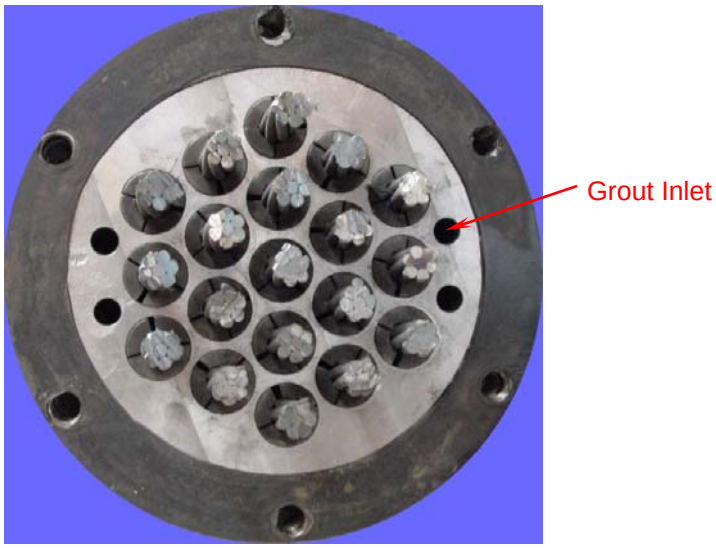

Figure 3-30: Anchor Head Orientation –Specimen #1

The spring plate was not used during the initial stressing of each strand. This resulted in unequal wedge seating on some of the strands at the deck end, shown in Figure 3-31. The wedges were marked after this was noticed. No movement of the wedges during the final stressing or the fatigue test was

observed. The use of the spring plate during the initial stressing of specimen #2 was a result of the observations made during initial stressing of stay cable specimen #1.

Figure 3-31: Unequally Seated Wedges

The grout for specimen #1 consisted of ordinary Type I Portland cement and tap water. The water cement ratio was 0.42 and no anti bleed admixtures were used in the grout. Not using any anti-bleed admixture might have been an additional factor for the grout void at the tower end.

A grout pump from VSL International was rented for the grouting operation. The pump was first shut off before the valves at the top and the bottom of the stay cable specimen were shut. This means that the stay was not further pressurized, which might also be an additional factor for the grout void at the tower end. The grout was cured for 10 days before the fatigue test was started.

3.3.3 Details of Specimen #2

The anchor head was orientated with the grout inlet and outlet at the top and bottom of the anchor head as shown in Figure 3-32. This orientation resulted in a fully grouted specimen without any major voids. However, it is unclear whether the orientation of the grout ports is the only reason for the grout void which occurred in specimen #1.

Note that the hexagonal configuration of the strand results in equal moments of inertia around the vertical and horizontal axis of the stay, which means equal stiffness for specimen #1 and #2.

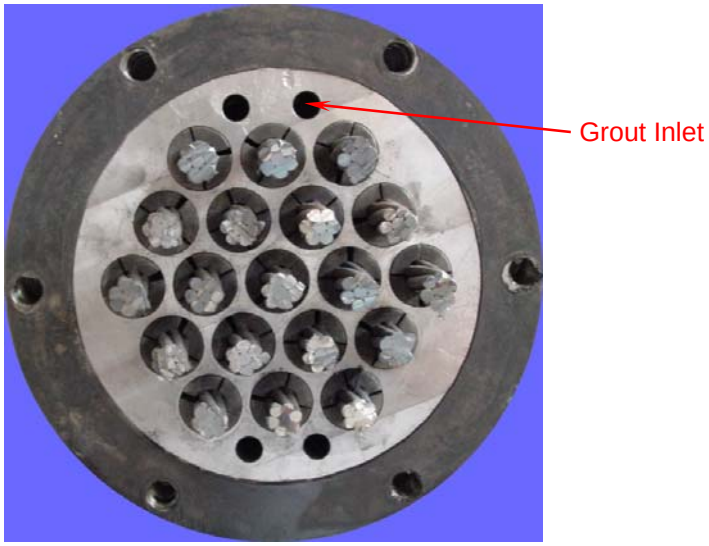

Figure 3-32: Anchor Head Orientation –Specimen #2

The grout for specimen #2 consisted of Type I Portland cement and tap water. The water cement ratio was 0.42 and an anti-bleed admixture (Sikament 300 SC) with a dosage of 2.2% was used for the grout. The installation of the

specimen was performed exactly as described and the grout pump owned by FSEL was used for the grouting. The grout was cured for 21 days before the fatigue test was started.

3.4 FATIGUE TEST

The test frame with the stressed and grouted specimen was placed under the test ram and bolted to the lab floor at both ends with temporary anchors. The clamp was attached to the test ram and to the stay cable specimen under the loading point at mid-span. The neutral level of the specimen was then determined by finding the displacement level of the ram that corresponding to zero load. The tests were performed under displacement control and the load was monitored using the controller unit of the ram.

Displacement at mid-span was then first applied manually. The specimen was pulled up at mid-span to the desired displacement and then pressed down, through zero to the desired negative displacement. The displacement amplitude was +/- 1.60 in. for specimen #1 and specimen #2. After performing this operation manually several times, the function generator of the controller was then used to impose the displacement as a sine wave with a defined frequency. The testing frequency was slowly increased from 0.1 Hz to the final testing frequency of 0.9 Hz for specimen #1 and 0.7 Hz for specimen #2. The testing frequency was controlled by the pumping capacity of the hydraulic system. The fatigue test was performed continuously for roughly 2,800,000 cycles for specimen #1 and specimen #2.

The specific testing parameters such as displacements, frequency, exact number of cycles and the testing period for the two stay cable specimens are given in Table 3-6 and Table 3-7.

Very stringent error limits were also set over the controller to ensure a well-defined test. If a certain limit was exceeded, the system shut off automatically and had to be restarted manually.

Table 3-6: Test Parameters of Specimen #1

Test Ram Amplitude:	+/- 1.60	in.	+/- 40.6	mm
Frequency:	0.9 Hz			
Total Number of Cycles:	2,808,398			
Grouting:	Time:	11.00 am	Date:	02/26/01
Fatigue Test Started:	Time:	5:30 pm	Date:	03/08/01
Fatigue Test Ended:	Time:	10:00 pm	Date:	04/15/01

Table 3-7: Test Parameters of Specimen #2

Test Ram Amplitude:	+/- 1.60	in.	+/- 40.6	mm
Frequency:	0.7 Hz			
Total Number of Cycles:	2,865,103			
Grouting:	Time:	11.00 am	Date:	06/01/01
Fatigue Test Started:	Time:	3:00 pm	Date:	06/22/01
Fatigue Test Ended:	Time:	10:45 am	Date:	08/09/01

3.5 SOUNDPRINT - ACOUSTIC MONITORING

Soundprint (Pure Technologies Ltd.) provided 4 acoustic transducers and all the required hardware shown in Figure 3-33 for acoustic monitoring of the specimen. The data obtained during testing were downloaded over the Internet, processed, and made available to the research team on the company's web page.

Figure 3-33: Soundprint Instrumentation and Acoustic Sensor

The 4 transducers were mounted to the stay cable specimen using epoxy. The sensors were placed on both anchor heads and along the free length as shown in Figure 3-34. The transducers along the free length were placed directly on the tension rings for the first specimen. Because of poor acoustic coupling, the sensors were placed directly on the PE pipe for the second specimen.

The transducers were set up in a trigger mode, which was calibrated to detect wire breaks on the stay cable specimen. Soundprint calibrated its system on the first stay cable specimen. The UT research team performed the necessary impact calibrations for the second specimen. The system allowed for a specific time stamp for each event, such as anchorage noises and wire fractures. Furthermore the location of the event was also reported. This information allowed

for a preliminary idea of the location and number of breaks accumulated during the fatigue test. The system was also used for pluck tests of the stay cable. The pluck tests were performed to obtain natural frequency data of the specimen.

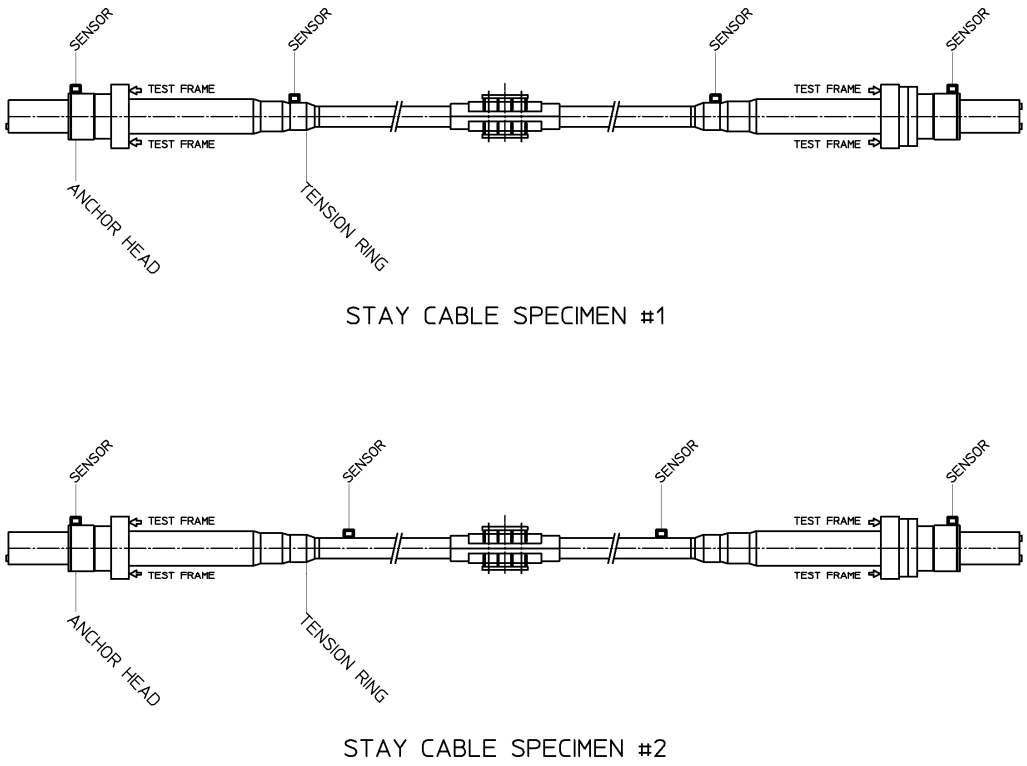

Figure 3-34: Location of Soundprint Sensors

CHAPTER 4
Fatigue Test Results

This chapter presents the results and observations made during the post-mortem investigation of two full-scale fatigue tests. The condition of the grout, location and description of wire breaks and stiffness data are presented.

4.1 METHOD OF OPENING THE SPECIMENS AND NOMENCLATURE

After the fatigue test was performed, the ram was disconnected and a post mortem investigation (autopsy) was performed. The specimen was cut into five 7-ft (2.1-m) segments in two steps: first a 1-in. (25-mm) ring was cut out of the PE pipe using a router, and then the grout and strand were cut using a disc grinder as shown in Figure 4-1.

Figure 4-1: Cutting of the Specimen

A nomenclature for the strands and the wires was established as shown in Figure 4-2 and Figure 4-3. The strands were numbered from #1 to #19 and the wires from #1 to #7, with #7 being the center wire.

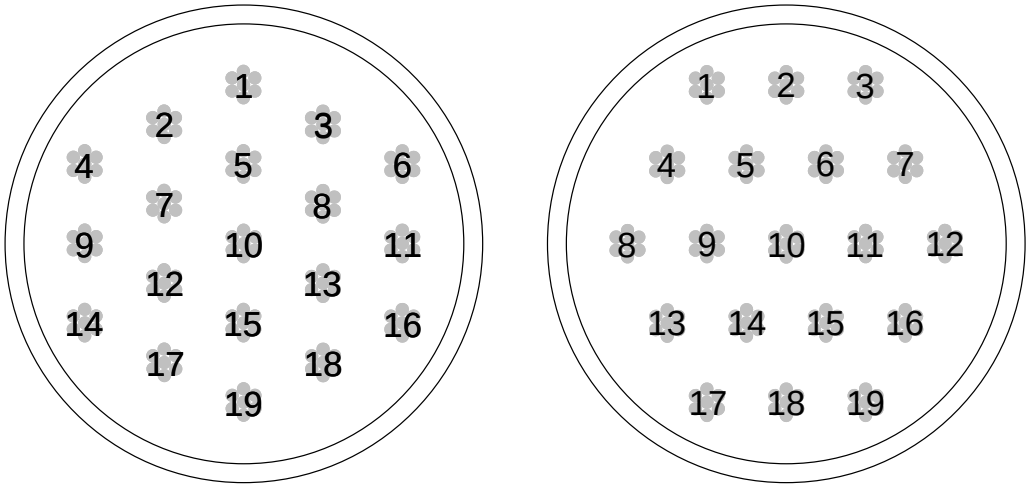

Specimen #1 Specimen #2

Figure 4-2: Nomenclature for the Strands

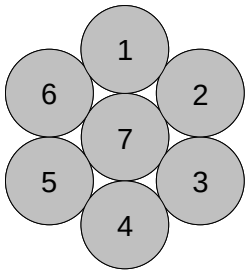

Figure 4-3: Nomenclature for the Wires of a Strand

4.2 GROUT CONDITION

4.2.1 Specimen #1

The grout for specimen #1 consisted of ordinary Type I Portland cement and tap water. The water cement ratio was 0.42 and no admixtures were used in the grout. The grouting operation was performed as described in Chapter 3.

Large amounts of bleed water were observed on all 6 test-cubes that were taken at the end of the grouting operation. Figure 4-4 shows the bleed water that had accumulated at the surface of the 2 x 2 x 2 in. (50 x 50 x 50 mm) test cube about one hour after the grouting operation. The bleed water had evaporated 12 hours after the cubes had been cast and a solid coupon remained. The discharge of bleed water resulted in test coupon with dimensions of 2 x 2 x 1.75 in. (50 x 50 x 45 mm). The surface of the test coupons had no visual imperfections.

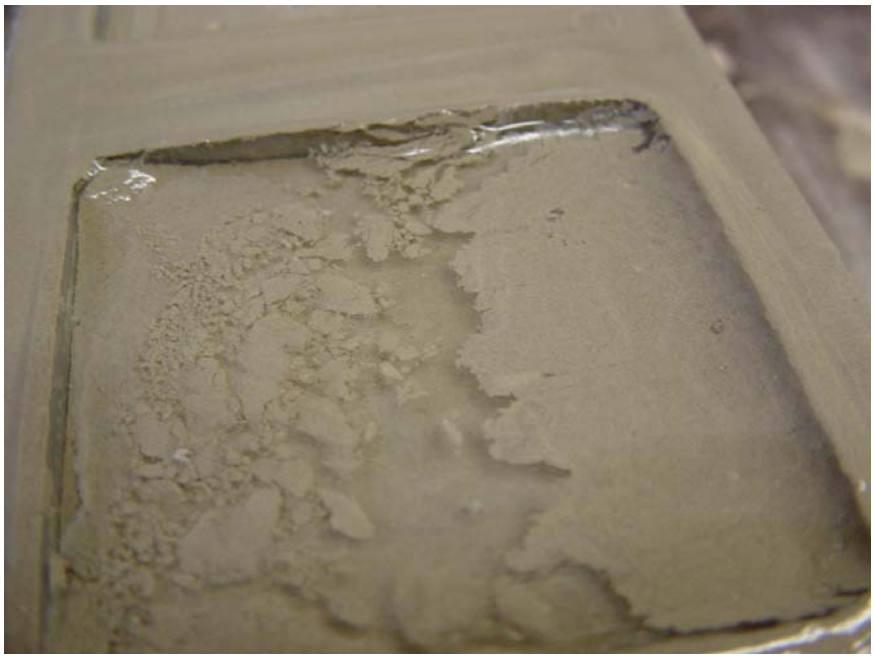

Figure 4-4: Bleed Water on the Surface of a Test Cube

After the fatigue test, the specimen was examined. Figure 4-5 shows a large grout void that was found at the tower anchorage, which was the elevated point during the grouting operation. It had a length of roughly 20 in. (500 mm) and a maximum depth of 1.5 in. (40 mm).

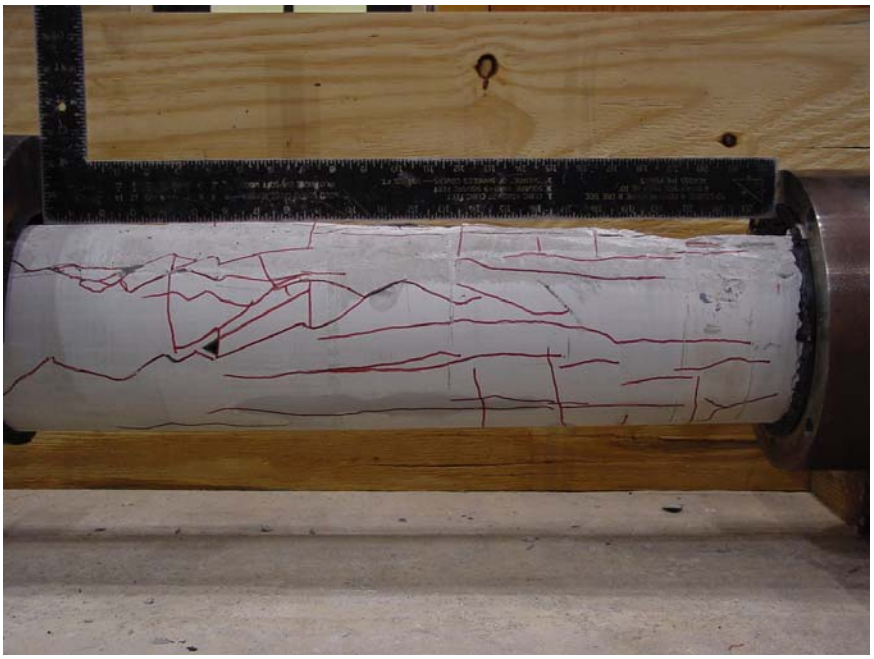

Figure 4-5: Grout Void at the Tower Anchorage – Specimen #1

Strands #1 and #2 were fully exposed within the grout void as shown in Figure 4-6. A very thin layer of grout covered strands #3 and #4. The exposed lengths of #1 and #2 were roughly 12 in. (300 mm).

It is unclear whether strands #1 and #2 were in contact with grout at some point during the grouting operating. The openings in the anchor head for strands #1 and #2 were fully grouted, as shown Figure 4-6, which might be an indication that the entire stay cable was fully grouted at some point and that the grout void is a result of a bleed-water concentration at the top end of the stay cable. The bleed water found on test cubes indicates that the occurrence of bleed water was also

likely at the elevated point (tower anchorage) of the stay cable specimen. Occurrences of bleed water and a grout void at the elevated point would indicate that the exposed strands found within the void were at one point fully or partly surrounded by bleed water. It is also possible that the grout found in the opening for the strands in the anchor head was grout that returned from the grout cap through the openings.

However, no significant signs of corrosion were found on the exposed strands in the grout void or on the anchor head. The surface corrosion seen in Figure 4-6 is light surface corrosion that was found on the shim plate. The location of the light corrosion would point to crevice corrosion in this area where the surfaces of the shim plate and the threaded nut are in direct contact.

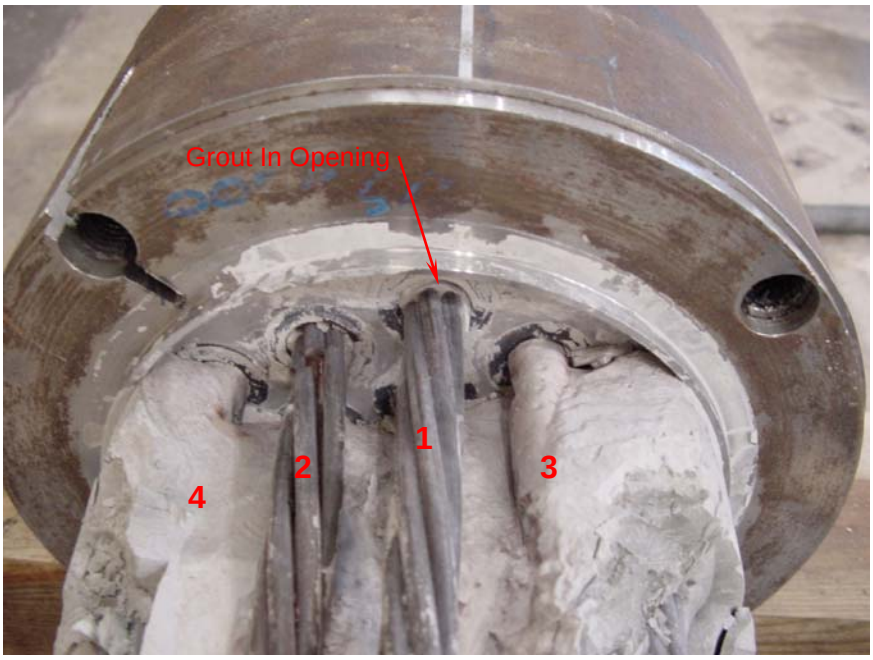

Figure 4-6: Exposed Strand within a Grout Void – Specimen #1

The grout in the rest of the specimen was homogeneous and only minor surface defects were found. The defects were often very close to the helical spacer wire as shown in Figure 4-7. Orange surface corrosion was found on some locations at the very outside of the helical spacer wire where it was in contact with the PE pipe.

Figure 4-7: Grout Surface Defect and Corrosion on Helix – Specimen #1

Several windows were cut into the PE pipe during the fatigue test of specimen #1. Shortly after the windows were cut and opened, fine, parallel, transverse cracks formed in the grout within the windows as seen in Figure 4-8. These fine hairline cracks are due to shrinkage of the grout in the exposed area. Similar shrinkage cracks were found in all the windows that had been cut into the

actual stay cables of the Fred Hartman Bridge, shown in Figure 4-9. Similar cracking was found in earlier investigations on stay cables (Hamilton 1995).

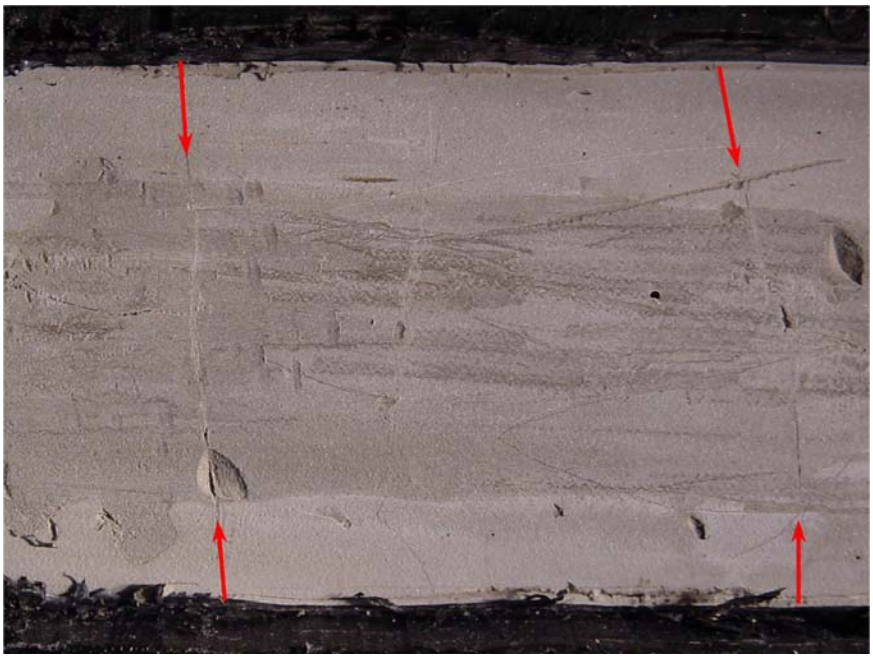

Figure 4-8: Transverse Grout Cracks – Specimen #1

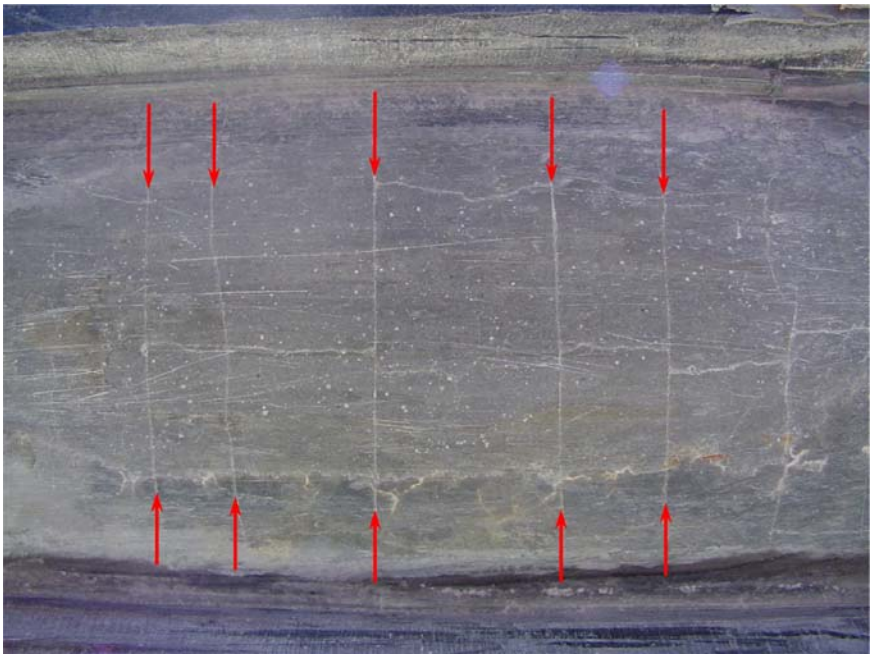

Figure 4-9: Transverse Grout Cracks - Fred Hartman Bridge

Longitudinal cracks in the grout were found wherever wire breaks occurred. Figure 4-10 shows the same view after the PE was removed and after some grout was chipped off. The longitudinal cracks were above a location where wire breaks occurred.

The location shown in Figure 4-10 is under the loading point at mid span of the specimen. At this location high curvature and high bending stresses occurred which might be an explanation not only for the occurrence of wire breaks, but also for the parallel cracks. Note that these cracks were seen immediately after the PE was removed, different from the shrinkage cracks described earlier.

Figure 4-10: Longitudinal Cracks and Corresponding Wire Breaks

4.2.2 Specimen #2

The grout for specimen #2 consisted of Type I Portland cement, tap water and an anti-bleed admixture (Sikament 300 SC) with a dosage of 2.2%. The water cement ratio was 0.42. It should be noted at this point that it was suggested later by Schokker (2001) to mix the admixture before it is added to the cement and water. Such a recommendation is not present in the usage guide that came with the Sikament 300 SC anti-bleed admixture. The admixture for specimen #2 was therefore not specially treated or mixed before usage.

No bleed water was found on grout samples and no major grout voids were found within the specimen after the fatigue test. As shown in Figure 4-11, closely spaced air voids were found at the deck anchorage. It was observed that an intense smell was emitted, similar to the one of the original admixture, when the PE pipe was opened during the autopsy of the stay cable specimen. It also appeared that it was much easier to chip the grout within a freshly opened section than a grouted section that had been open for a number of days before the grout was chipped. This would indicate that the grout gains strength as soon as the PE pipe is removed and the grout is exposed. However, no measurements were taken to verify the above-mentioned observation.

There were some localized signs of orange corrosion on some intact strands as well as some fine corrosion spots on the helical spacer wire. Figure 4-12 shows a typical spot of such strand and helix corrosion, which was found under the loading point at the side of the specimen.

Figure 4-11: Air Voids at the Deck Anchorage – Specimen #2

Figure 4-12: Localized Corrosion on Strand and Helix – Specimen #2

4.3 WIRE BREAKS

4.3.1 Specimen #1

A total of 25 wire breaks occurred during the first fatigue test and were also reported by Soundprint. The breaks can be grouped into two general locations, 14 breaks occurred at the tower anchorage, and 11 under the loading point (Figure 4-13).

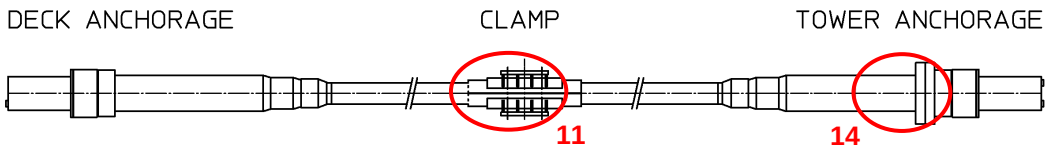

Figure 4-13: Wire Breaks Specimen #1

The number of cycles between the individual failures based on Soundprint (see Section 4.6) is shown in Figure 4-14. The first break occurred at 300,000 cycles, where after wire breaks occurred in intervals between 10,000 and a maximum of 240,000 cycles. The fatigue test was stopped after 2,808,398 cycles.

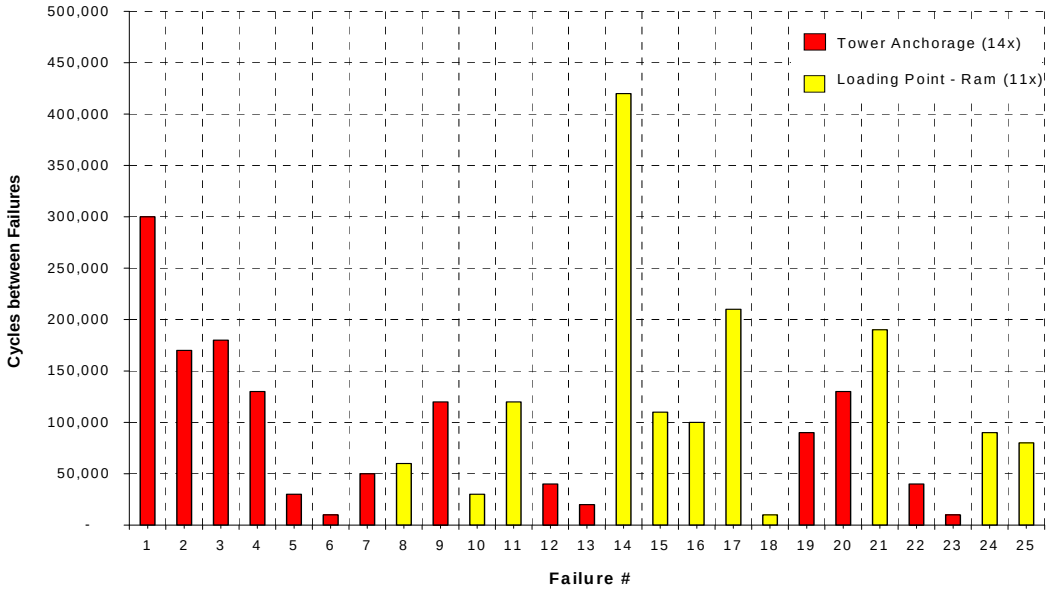

Figure 4-14: Cycles between Failures (based on Soundprint) – Specimen #1

All breaks at the tower anchorage occurred within 14 in. (355 mm) of the front face of the anchor head. The 14 wire breaks occurred in strands #1, #2 and #19 – the strands that are on the top and bottom of the specimen as shown in Figure 4-15. The top and bottom fibers are expected to have the highest bending stress ranges in a bending test.

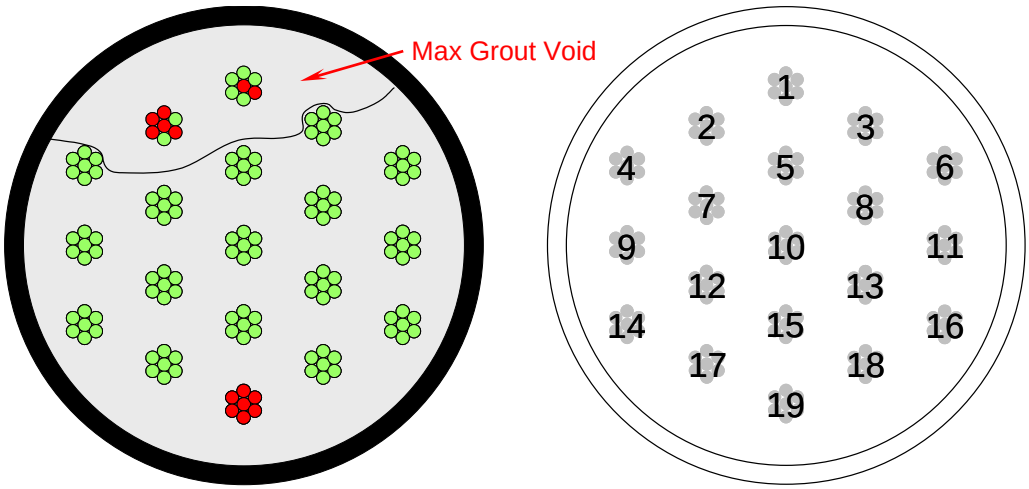

Figure 4-15: Wire Breaks at the Tower Anchorage – Specimen #1

All the breaks on strand #2 and one break on strand #1 occurred within the grout void at the tower anchorage. One of the breaks on strand #1 and all the breaks on strand #19 were within the fully grouted region.

Figure 4-17 shows the longitudinal location of the wire breaks. Two of the total of 6 breaks that occurred within the grout void occurred just past the anchor head. The strands that were fully exposed within the grout void where surrounded by grout and therefore confined within the opening in the anchor head. All 7 breaks on strand #19 occurred just inside of the threaded nut. Within the threaded nut the PE Pipe is threaded into the nut that stiffens the stay cable. A close up of this region is shown in Figure 4-16.

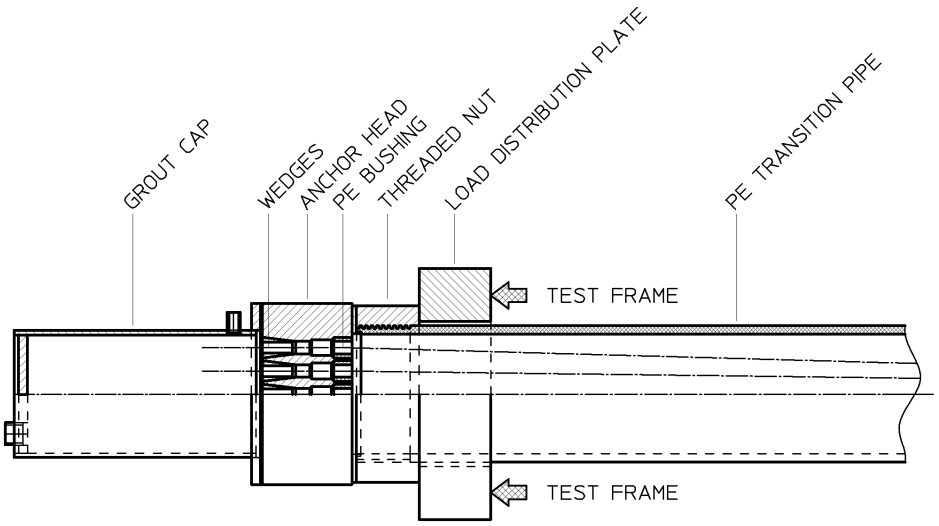

DECK ANCHORAGE

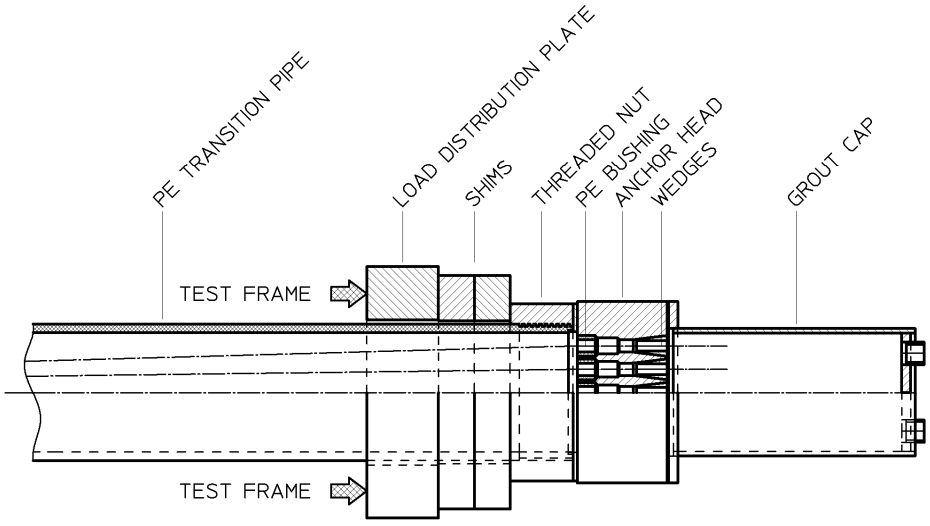

TOWER ANCHORAGE

Figure 4-16: Anchorage Detail

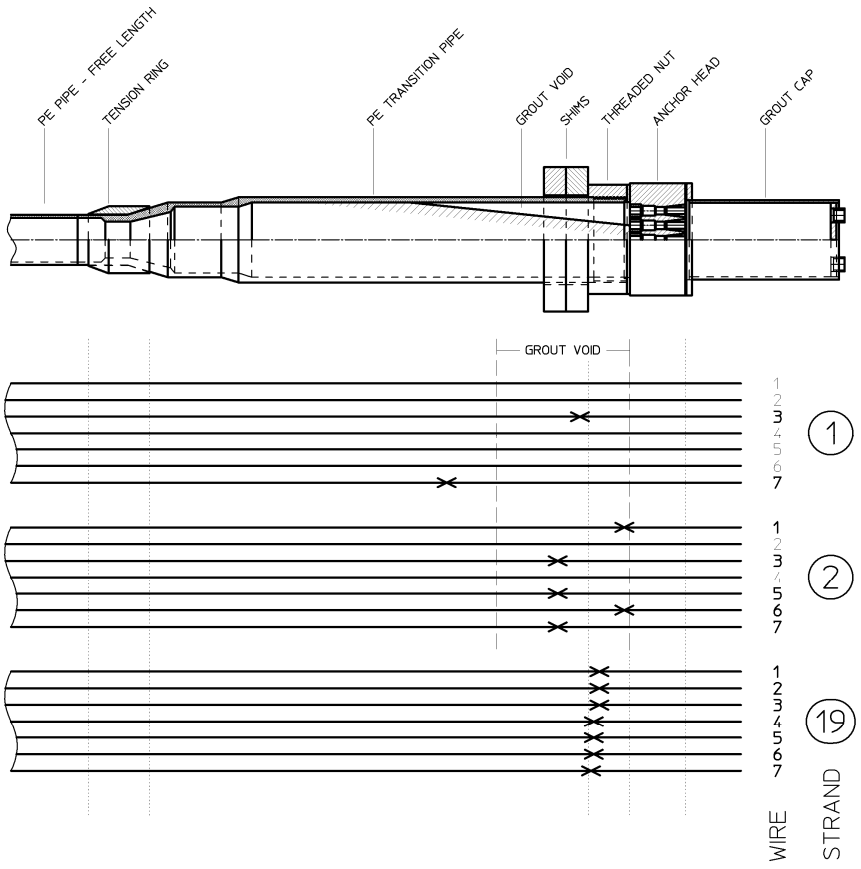

Figure 4-17: Wire Breaks at the Tower Anchorage – Specimen #1

All 9 breaks so far described occurred where the entire specimen or an individual strand experienced a relatively sudden change in confinement. This might be an indication that these are areas with localized high curvatures and therefore high bending stresses which might have led to the fatigue fractures. The 3 remaining breaks on strand #2 occurred roughly 5 in. (130 mm) outside of the front face of the anchor head within the void. The remaining break on strand #1 occurred on the center wire outside of the grout void, 14 in. (355 mm) from the front face of the anchor head.

Under the loading point, the 11 wire breaks occurred on strands #1 and #19 (Figure 4-18). Interestingly, both strands also experienced fractures in the tower anchorage region. All breaks were located in a 23 in. (580 mm) window, with a bias towards the deck anchorage side (Figure 4-19).

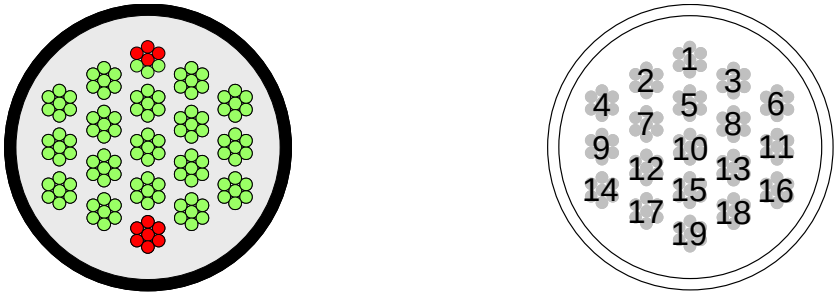

Figure 4-18: Wire Breaks under the Loading Point – Specimen #1

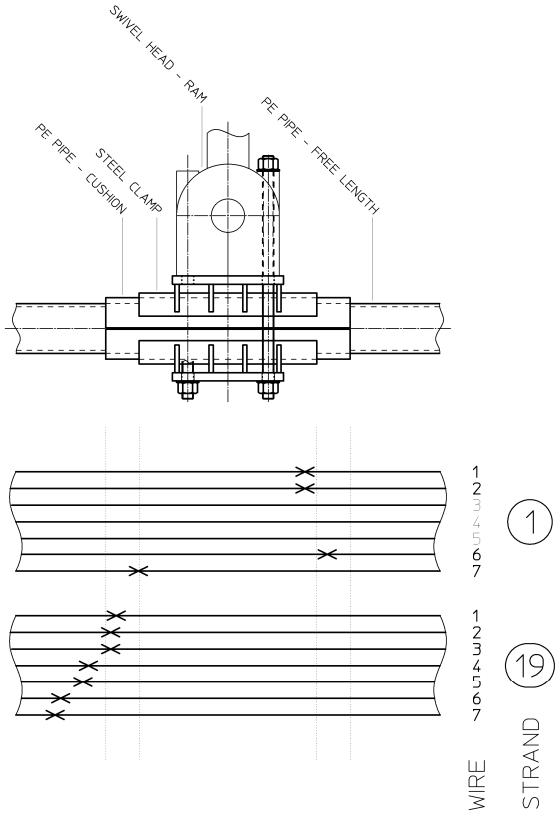

Figure 4-19: Wire Breaks under the Loading Point – Specimen #1

The wire fractures that occurred on strands within the grout void at the tower anchorage of stay cable specimen #1 do not show any signs of corrosion. Figure 4-20 shows the wire fractures that occurred on strand #2 at the tower anchorage.

Figure 4-20: Wire Breaks – Strand #2 – Tower Anchorage – Specimen #1

The area immediately around the wire breaks on strand #19 at the tower anchorage showed orange surface corrosion (Figure 4-21). Looking at the fracture surfaces of strand #19 indicates that the fractures were a result of fretting fatigue. Fretting fatigue occurred because of the relative movements of the individual wires within the same strand. A clear circular fatigue crack that was initiated at a contact point with another wire can be found on all the wires of strand #19. Figure 4-22 shows a close up of the fractures on strand #19 where the fracture surfaces with the fatigue cracks and the points of initiation can be clearly identified. The orange corrosion seen on strand #19 might have helped to initiate the individual cracks or is a corrosion product that occurred after a wire fractured. After an individual wire fractured, the increased relative movement of a still intact wire and the sharp fracture surface of the broken wire might have increased surface abrasion that led to the observed corrosion/fretting products.

Figure 4-21: Wire Breaks – Strand #19 – Tower Anchorage – Specimen #1

Figure 4-22: Fracture Surface – Strand #19 – Tower Anchorage – Specimen #1

The fatigue crack surfaces on all the fractured wires in specimen #1 and #2 were initiated at contact points between individual wires. Some of the strands that experienced wire fractures showed signs of corrosion products only at the

contact point between the wires exemplified by the failure location of strand #1 under the loading point of specimen #1. Figure 4-23 shows the corrosion product on the inside of a wire that has fractured. The corrosion occurred mainly at the contact points between wires. Note that the same occurrence of corrosion on the inside at the contact points between the wires can also be seen on strand #19 in Figure 4-21.

Figure 4-23: Wire Breaks – Strand #1 – Loading Point – Specimen #1

4.3.2 Specimen #2

A total of 67 wire breaks were found during the autopsy of specimen #2, of which (63) were initially reported by Soundprint (see Section 4.6). The breaks

can be grouped into two locations, 51 breaks occurred at the tower anchorage and 16 under the loading point (Figure 4-24). Potentially there is 1 break at the deck anchorage as discussed later.

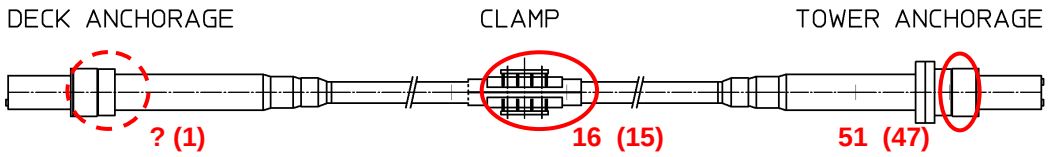

Figure 4-24: Wire Breaks Specimen #2

The number of cycles between the individual failures, detected by Soundprint, is shown in Figure 4-25. The first wire break occurred at 420,000 cycles, where after wire breaks occurred in intervals between 1 and a maximum of 210,000 cycles. The fatigue test was stopped after 2,865,103 cycles.

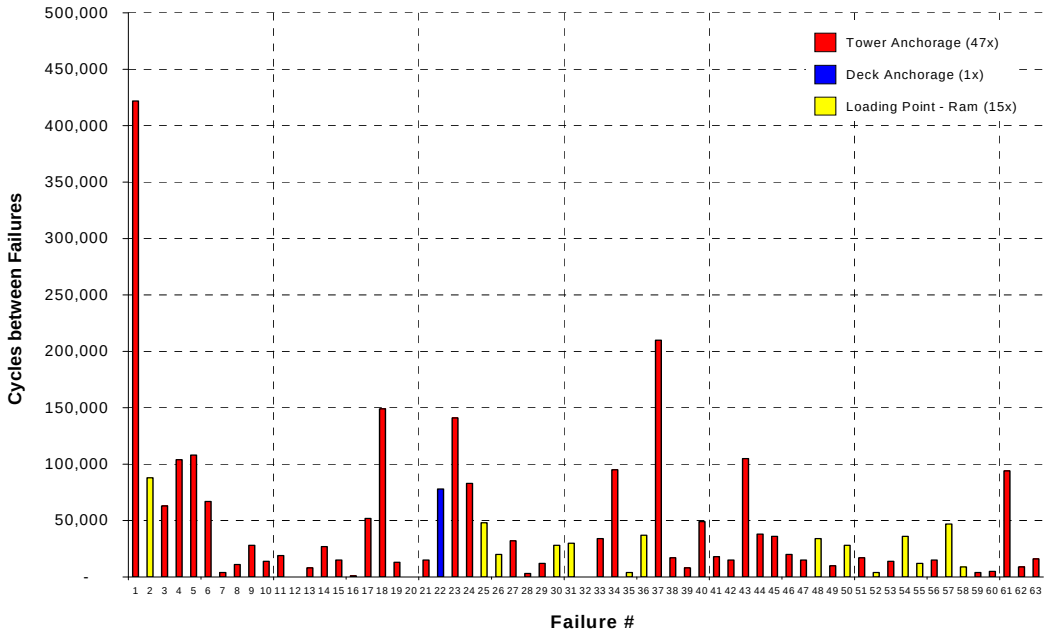

Figure 4-25: Cycles between Failures (based on Soundprint) – Specimen #2

Most of the fractures at the tower anchorage occurred within the anchor head and not more than 3.25 in. (80 mm) from the front face of the anchor head.

The 51 wire breaks occurred on 10 different strands which are mainly at the very top and bottom of the specimen as shown in Figure 4-26.

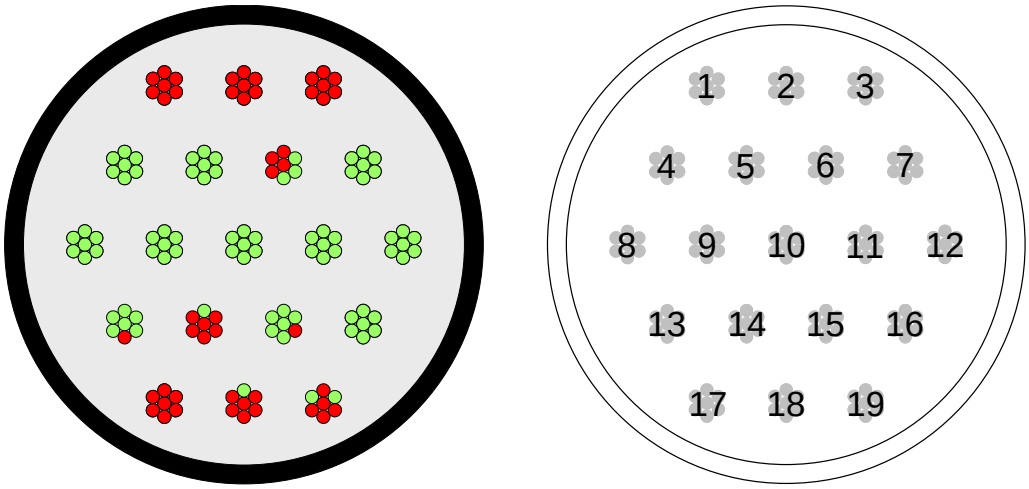

Figure 4-26: Wire Breaks at the Tower Anchorage – Specimen #2

Figure 4-27 shows the longitudinal location of the wire breaks. All the breaks on strands #1, #3, #13, #14, #15, #18, and #19 and one break on strand #2 occurred within +/- 1.5 in. (+/- 40 mm) of the front face of the anchor head (transition between the anchor head and the grouted PE pipe). The breaks on strand #19 and the remaining 6 breaks on strand #2 occurred before the wedges. It should be noted that the fractures were not initiated at the teeth marks from the wedges, but just outside of the actual gripping area as shown in Figure 4-31. The remaining 4 breaks occurred on strand #6 just inside the region where the PE pipe is still surrounded and stiffened by the threaded nut.

Once again, the breaks occurred at locations where the entire specimen or an individual strand experienced a relatively sudden change in confinement. This kind of behavior was also observed on specimen #1 as noted earlier although no fractures were found within the anchor head in specimen #1.

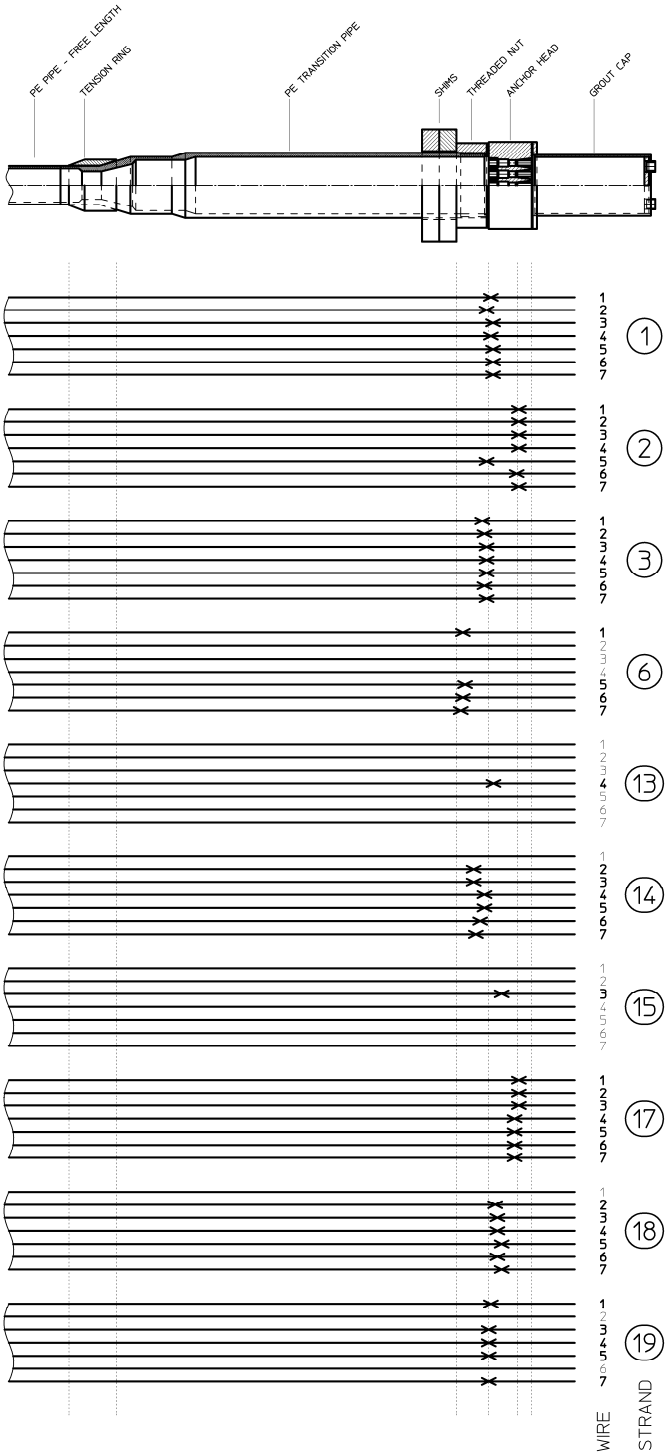
PE PIPE - FREE LENGTH
TENSION RING
PE TRANSITION PIPE
SHIMS
THREADED NUT
ANCHOR HEAD
GROUT CAP
1
2
3
4
5
6
7
WIRE
STRAND

Figure 4-27: Wire Breaks at the Tower Anchorage – Specimen #2

Under the loading point, the 16 wire breaks occurred on strands #17 and #18. Both these strands are at the outer fibers of the cross section, which is an observation that has been made on all failure locations so far. However, strands #17 and #18 are both strands that are on the bottom of the specimen, which results in an unsymmetrical distribution of the failure locations as shown in Figure 4-28. It should also be noted that both these strands experienced wire fractures in the tower anchorage region. The occurrence of wire breaks under the loading point and at the tower anchorage on the same strand is an observation that has already been made on specimen #1.

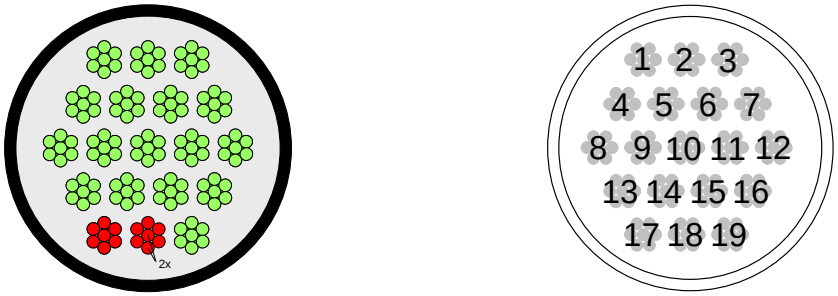

Figure 4-28: Wire Breaks under the Loading Point – Specimen #2

All breaks were located in a 10.25 in. (260 mm) window under the loading point, with a slight tendency towards the tower anchorage side. Thirteen breaks were found very localized within +/- 3.25 in. (+/- 80 mm), and 3 breaks occurred roughly 8.5 in. (215 mm) away from the main failure locations towards the deck side. Interestingly, wires #4 and #7 of strand #18 experienced two fractures within the same strand as shown in Figure 4-28 and Figure 4-29. The second location of the wire breaks is an area where a strand, specifically the bottom wire of the strand, might have been in contact with the helical spacer wire. However, as shown later, it is not believed that the fracture initiated by fretting against the helical spacer wire.

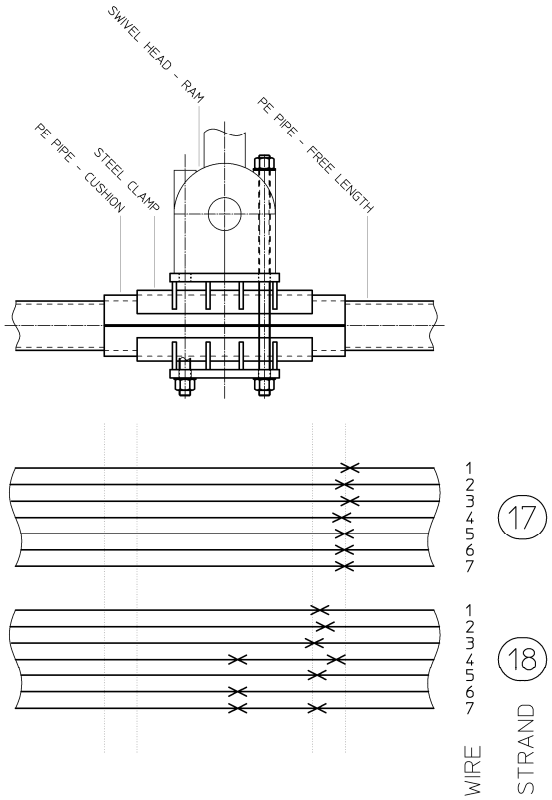

Figure 4-29: Wire Breaks under the Loading Point – Specimen #2

Soundprint reported one wire break at the deck anchorage, roughly 18 in. (500 mm) from the anchor head. The grout has been completely removed in an area of +/- 12 in. (+/- 300 mm) around the predicted failure location and no breaks were found on the 6 outside wires of the each strand. In addition, the 6 strands at the extreme fibers have been removed in the same area and have been completely unwound to be able to inspect the center wire. However, no breaks were found on these 6 center wires. The strands have not been inspected in the anchor head region at this point. Note, Paulson (2001) indicated that the reported event was very likely a wire break, although there is the possibility that it was a strand that slipped at the wedges.

The wire fractures that occurred on specimen #2 are generally very similar to the ones already seen on specimen #1. Classical and representative examples are the breaks on strand #2 of specimen #2 are shown in Figure 4-30. The fracture surfaces with the fatigue cracks and the points of initiation can be clearly identified in this figure. The breaks shown are also very similar to the failures on strand #19 of specimen #1, which have been discussed earlier.

Figure 4-30: Fracture Surfaces – Strand #1 – Tower Anchorage – Specimen #2

Other failure locations are the breaks that occurred just past the wedges. It has been mentioned earlier that the breaks in this region were not initiated by one of the teeth marks on the wires caused by the wedges. The breaks occurred just outside the gripping area as shown in Figure 4-31. Figure 4-32 indicates that all the breaks were initiated at contact points with the center wire and none of the fractures appears to have been initiated from the outside surface of the strand. The failures on strand #17 that also occurred just outside of the wedges show an almost identical behavior in terms of fracture initiation and location of the breaks.

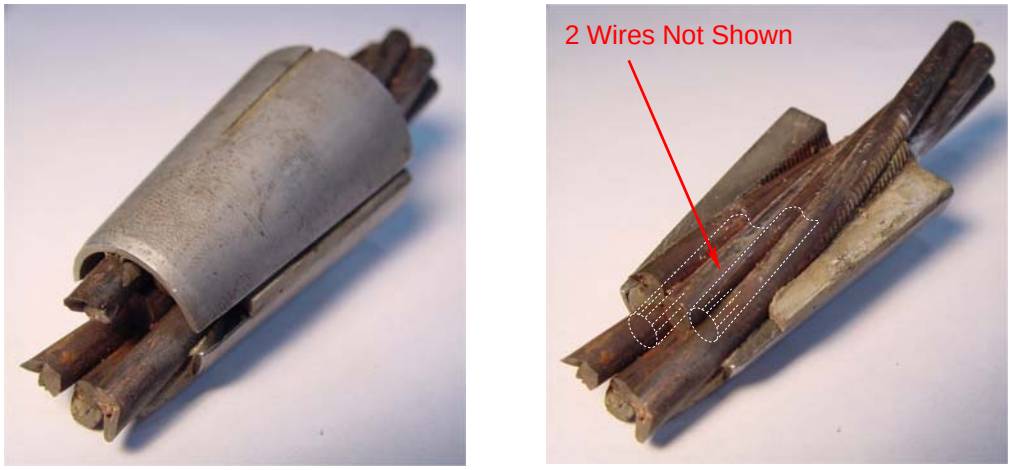

Figure 4-31: Opened Wedges and Wire Fractures – Strand #2 – Specimen #2

Figure 4-32: Fracture Surfaces – Strand #2 – Tower Anchorage – Specimen #2

One of the fractured wires under the loading point of specimen #2 was found near a possible contact point with the helical spacer wire as shown in Figure 4-33. Looking at the fracture surface (Figure 4-34) of the particular wire indicates however, that the fracture was initiated at the contact point with the center wire, which was also fractured. The fatigue crack is also significantly larger than on all other failure locations, which indicates that the tension in the

strand was negligible at the time of fracture. Consequently, this fracture was the second fracture that occurred on this particular wire.

Figure 4-33: Wire Break Close to Helical Spacer – Specimen #2

Figure 4-34: Fracture Surface – Specimen #2

4.3.3 Wire Break Summary

A total of 92 wire breaks occurred on 17 different strands during the two fatigue tests. The breaks were very localized at the tower anchor head and under the loading point. The breaks at the tower end mainly occurred in regions where the cable or a strand experienced a sudden change in confinement, for example the transition zone between anchor head and the grouted PE pipe, the end of the threaded nut or just before the gripping area at the wedges.

As expected in a bending fatigue test, all the breaks occurred at the outer fibers of the cable cross-section where the bending stress ranges are highest. The orientation of the strands was different for the two specimens as described in Chapter 3. However, assuming a fully composite cross section, both specimens have the same moment of inertia and therefore stiffness. The maximum outer fibers of specimen #1 are on strands #1 and #19 and are 2.9 in. (74 mm) away

from the neutral axis of the stay. The outer fibers of specimen #2 are on strands #1, #2, #3, #17, #18, and #19 and have a maximum distance of 2.5 in. (64 mm) from the neural axis.

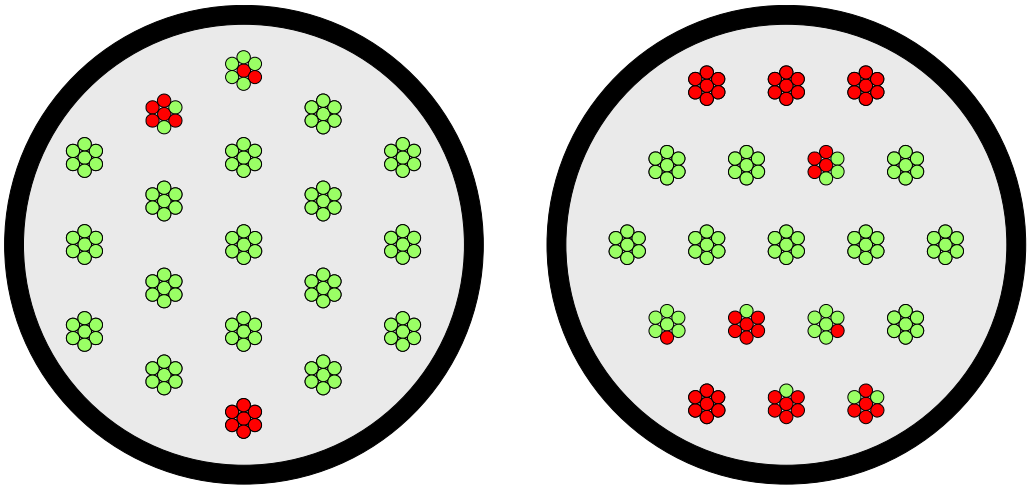

Figure 4-35: Strand Orientation and Wire Breaks for Specimen #1 and #2

The first wire fracture on specimen #1 occurred after 300,000 cycles, compared with 420,000 cycles on specimen #2. The difference in the number of cycles until the first wire break occurred is very small. One might argue that because of the orientation of the strands, the outer fibers of specimen #1 are likely to experience a higher stress range compared with specimen #2. The higher stress range would lead to an earlier initiation of a fatigue crack, and therefore earlier wire fracture on the outer fibers of specimen #1.

At the tower anchor head, 14 wire breaks occurred on specimen #1 and 51 on specimen #2. There are 6 strands exposed to the maximum bending stress in specimen #2 and 2 in specimen #1. This indicates that once the critical number of cycles is reached, 2 strands are susceptible to wire fracture in specimen #1 compared with the 6 in specimen #2. This argument might at least partly explain the difference in the number of wire breaks.

The breaks under the loading point are certainly breaks that occurred because of the way the test was performed and no direct conclusions about the bending fatigue behavior of a real stay cable in the free length should be made. Note that all strands that experienced wire fractures under the loading point also experienced fracture at the tower anchorage. This is an indication that the failures under the loading point did not have an influence on the test results.

Figure 4-36 and Figure 4-37 show the cumulative number of wire breaks under the loading point and at the tower anchorage versus the number of cycles. Note that there is a reasonably constant rate of occurrence of wire breaks once the first break was initiated. The data from the two specimens under the loading point compare very well for a fatigue test. The data at the tower anchorage are similar below 800,000 cycles. After roughly 800,000 cycles, the number of failures on specimen #2 starts increasing drastically, which might be because of the larger number of strands exposed to a relatively higher stress range.

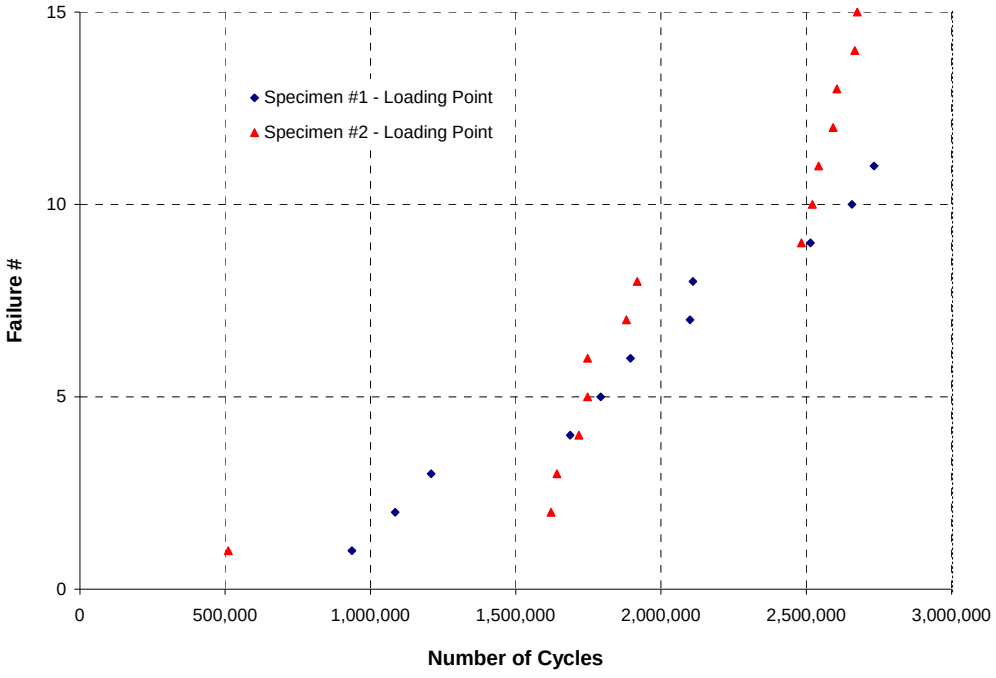

Figure 4-36: Cumulative Number of Failures vs. Cycles – Loading Point

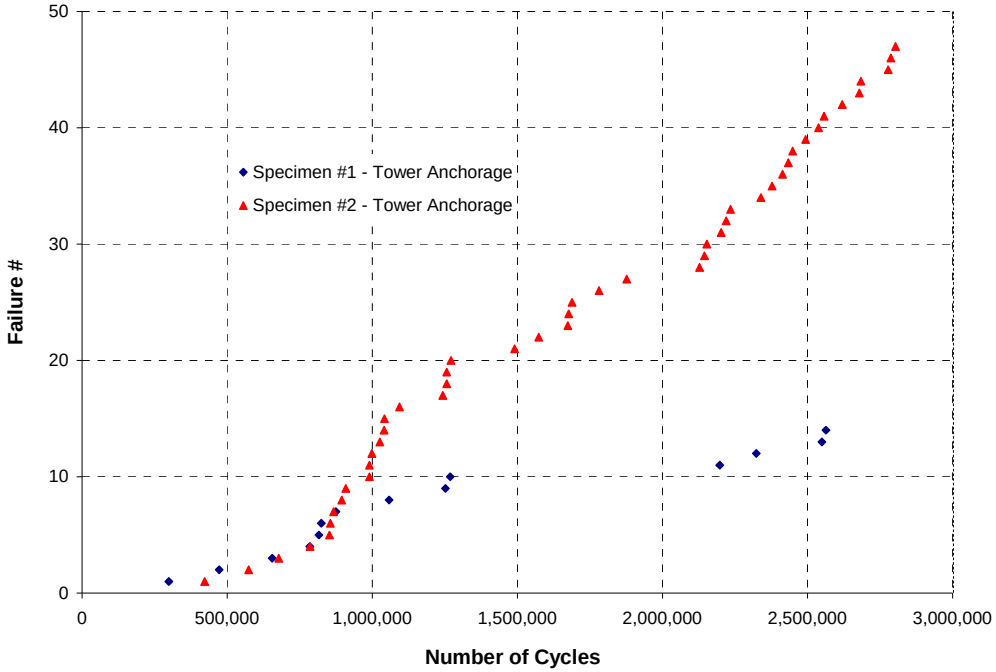

Figure 4-37: Cumulative Number of Failures vs. Cycles – Tower Anchorage

As mentioned earlier, the fracture surfaces indicated that most of the breaks were initiated at the contact points of the outer wires with the inner wire and some on contact points between the outer wires. It was observed that on 16 of the 18 strands that experienced fracture, the center wire was also found fractured. This does not necessarily indicate that the center wire was the first wire that fractured. This might indicate that the stresses at the points of contact were much higher than the pure axial and bending stresses or the contact stresses between the outer wires and the grout.

The biggest open question is why potentially only one break occurred at the deck anchorage of specimen #2 at 1,350,000 cycles. The specimens are 4 in. (100 mm) longer on the tower side, which would theoretically result in a slightly lower bending moment at the tower end. The difference in length is because of the

shim plates at the tower end. However the vast majority of the breaks still occurred at the tower end. The other differences between the ends of the specimens are that the tower anchorage was the elevated point during the grouting operation and that the cable was tensioned from the tower end, making the deck anchorage the dead end. Beside the above-mentioned irregularities, the specimens were symmetrical about the loading point.

It also appeared that the grout void did not influence the fatigue life significantly because the breaks still occurred in the same basic area. It has to be noted however that exposed strands within a void are a potential corrosion risk on actual bridge cables.

4.4 CHANGE IN STIFFNESS

The fatigue test on the two specimens was performed under displacement control. Generally, a reading of the current peak-to-peak loads required to get to the desired displacement was taken manually once a day over the entire testing period.

Figure 4-38 and Figure 4-39 show the peak loads to get to the required displacement versus number of cycles. The average of the forces for the upward and the downward forces can be reasonably approximated as a straight line for specimen #1 and a quadratic curve fit for specimen #2 as shown Figure 4-40 and Figure 4-41.

The accelerated reduction in stiffness observed on specimen #2 might be related to the larger number of failures that occurred during the test. It can be observed that the load to attain the displacement dropped significantly over the testing time, which indicates a reduction in stiffness. Both specimens showed a noticeable first drop in stiffness after the first couple of cycles.

Note that specimen #1 has a larger drop in load at the beginning compared with specimen #2. This first reduction is believed to be because of possible grout cracking and possibility further wedge seating. The loads started to reduce continuously after wire breaks started to occur. It should be noted that it was not possible to detect a single wire breakage event based on the reduction in stiffness. This is because the change in load after a wire break occurred was generally too small to detect reliability. However, certain individual wire breaks lead to a very significant change in load. This might be because these particular breaks were the last wires of a particular strand.

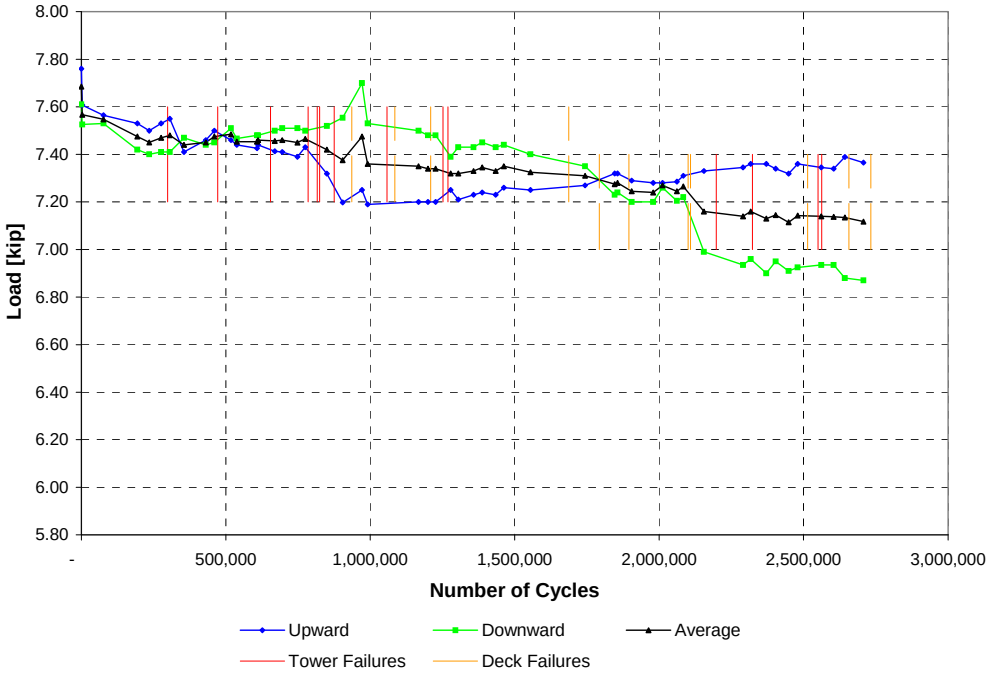

Figure 4-38: Number of Cycles vs. Load – Specimen #1

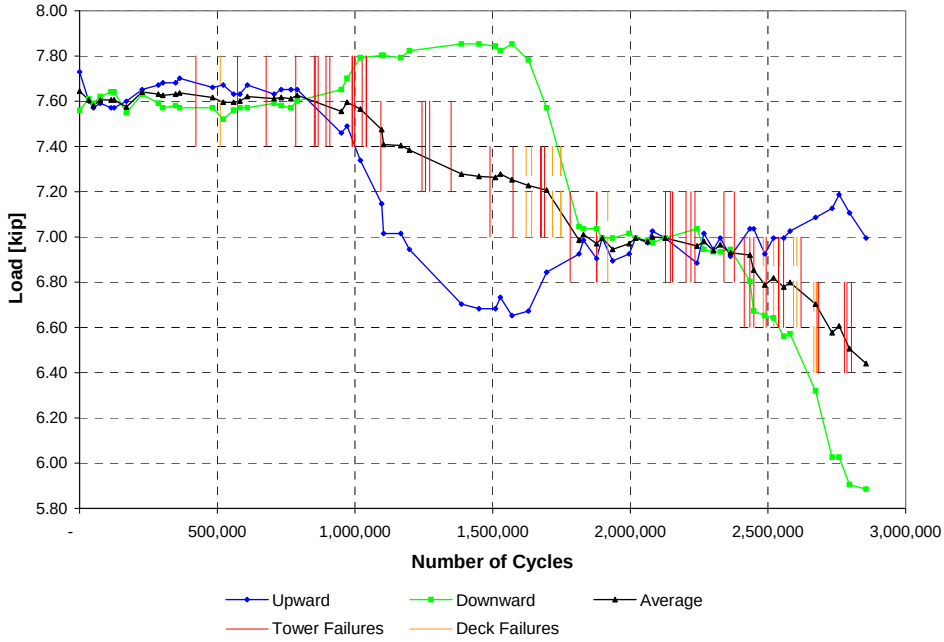

Figure 4-39: Number of Cycles vs. Load – Specimen #2

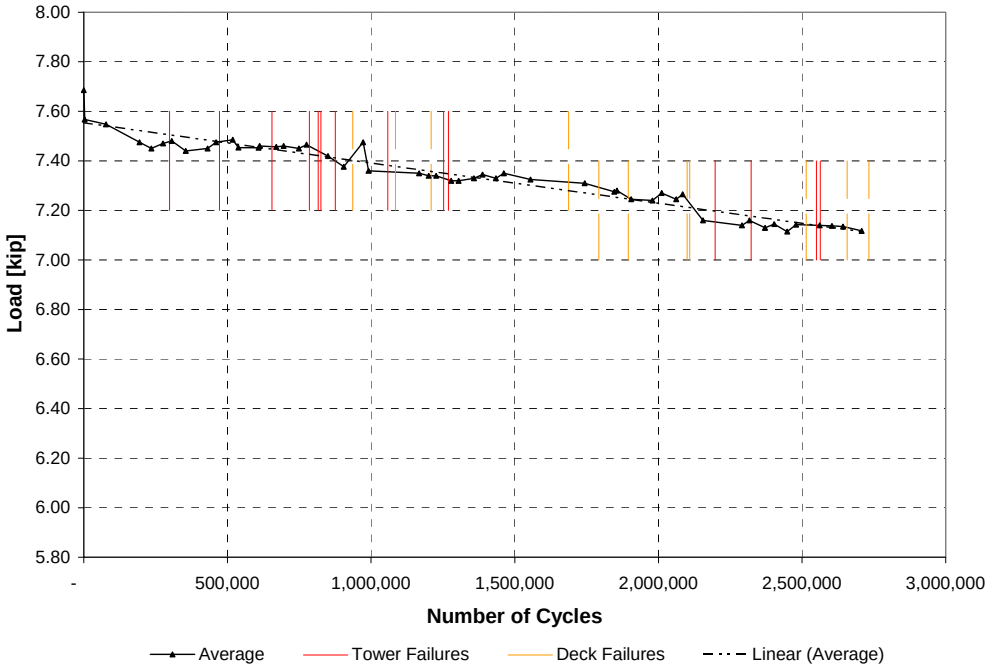

Figure 4-40: Number of Cycles vs. Average Load – Specimen #1

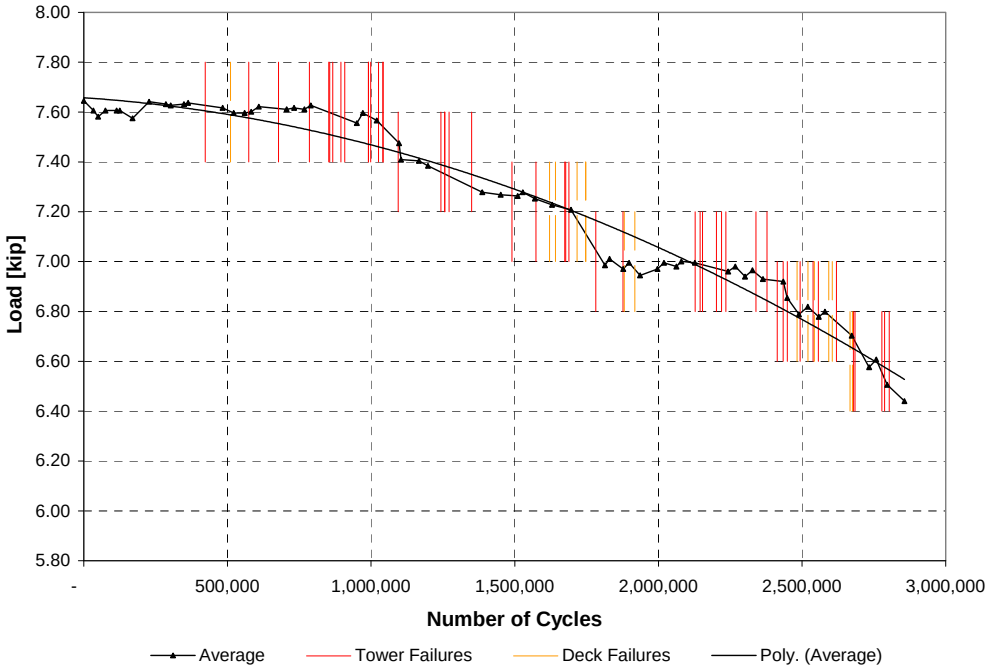

Figure 4-41: Number of Cycles vs. Load – Specimen #2

Interestingly, the required loads did not change equally on the upward and the downward movement. In fact, the force required to push down on the cable increased first, whereas the upward force required decreased at the beginning. This trend started to change after a number of breaks and the amount of force for the upward displacement started to increase, whereas the downward force stared to decrease. This behavior was observed on both specimens.

The unequal change in load between the upward and downward movement most likely occurred because the strands on the top failed first which led to an upward camber of the stay cable specimen. This behavior is similar to that of a concrete beam that is being post-tensioned.

4.5 PLUCK TEST

Pluck tests on the stay cable specimen were performed at the beginning and at the end of the fatigue test on specimen #2 and at the end of the fatigue test on specimen #1. They were used to determine the natural frequencies of the stay. The tests were performed by pulling up the specimen at mid-span with a weak link, a wire, which was attached to a pulling device – either the crane or the actuator used in the fatigue test (Figure 4-42). A sudden fracture in the link while the stay was continuously lifted led to free vibration. The estimated deflection of the cable specimen was roughly 0.75 in. (20 mm) just before fracture of the link occurred. The frequency data of the specimen were recorded using the 4 acoustic sensors provided by Soundprint. An FFT was performed to obtain the characteristic frequencies. The resulting natural frequencies for both specimens are given in Table 4-1. Based on the limited data, it is believed that the intact stay cable specimen has a natural frequency of roughly 12.5 Hz for the first mode.

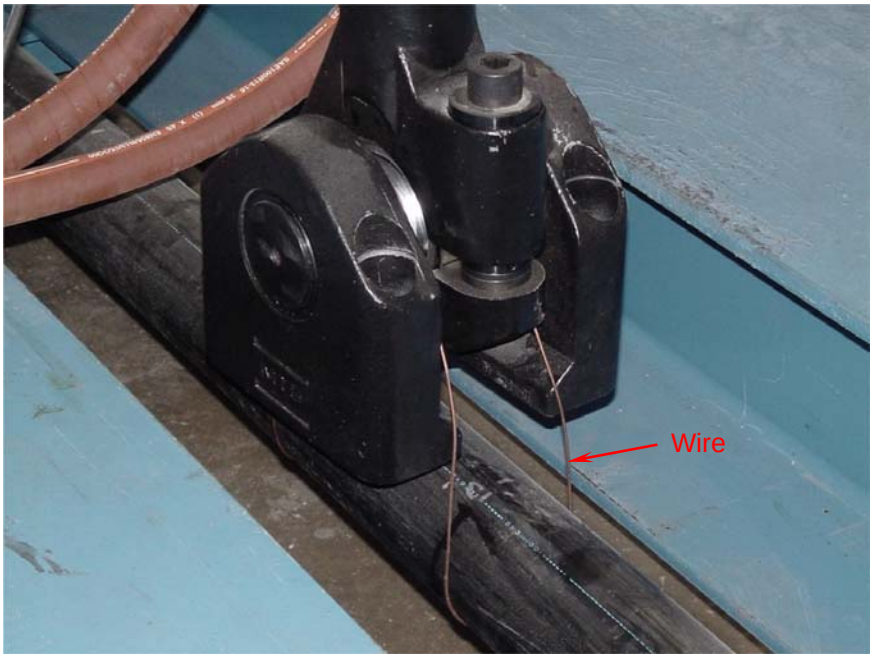

Figure 4-42: General Setup for a Pluck Test

The natural frequencies determined at the end of the test are lower because of the wire fractures that occurred during test. Every wire fracture lowers the tension force in the stay and therefore the frequency of the specimen. The difference in the frequency at the end of the test between the two specimens is because a larger number of wire breaks occurred on specimen #2.

Table 4-1: Natural Frequency

		1st mode	2nd mode
Specimen #1	Beginning	N/A	N/A
	End	12.0 Hz	24.0 Hz
Specimen #2	Beginning	12.5 Hz	25.5 Hz
	End	11.5 Hz	23.2 Hz

4.6 RELIABILITY OF THE SOUNDPRINT SYSTEM

The number of wire breaks reported by Soundprint was generally accurate. Of the 89 actual wire breaks that occurred during the two fatigue tests, 84 were detected and reported.

Note that Soundprint was notified that they might have missed 5 breaks on specimen #2. After a review, Paulson (2001) indicated that there were 4 breaks at the tower anchorage that had not been assigned to the database that was available to the UT research team. In addition, an extra break was reported in the free length close to the loading point. However, even without the update that was made, the reliability was considered to be good.

Because the reliability of the system was good, the data provided by Soundprint were generally used in the investigation. The time stamps for individual wire breaks, from which the number of cycles was determined, were found to be very useful in analyzing and presenting fatigue data.

Soundprint also provided the location of a wire break from the 3 sensors closest to the break. A location comparison, wire by wire, was not possible because the order that the wire breaks occurred could not be determined from the autopsy. However if one considers only the range in which wire breaks occurred, all the breaks were generally within a window of +/- 12 in. (+/- 300 mm) of the reported location.

CHAPTER 5
Comparison and Outlook

5.1 PERFORMANCE OF THE TEST SETUP

The two full-scale bending fatigue tests on stay cables described in this thesis were one of the first of its kind. The overall performance of the setup was very good, however, a few suggestions may be made for future modifications.

The clamping region was designed to reduce the stresses introduced to the specimen at mid-span to a minimum. However, both specimens experienced a number of fractures at this location. Considering the fact that all strands that experienced fractures at mid-span also experienced fractures at the anchorage, the failures under the loading may be called imperfections that do not influence the test results at the anchorage. A few modifications to the clamping setup have been recommended in Chapter 3.

The capacity of the actuator used for the two tests was chosen based on preliminary FEM. As it turned out, the estimated forces were too conservative which resulted in an oversized actuator. The testing frequency was thereafter only determined by the pumping capacity which resulted in a very long testing period for each specimen. The testing frequencies of 0.7 and 0.9 Hz represent the lower bounds of observed frequencies during vibration events on the Fred Hartman Bridge. However, studying possible dynamic effects at higher frequencies is a point of further investigation. Note that a smaller actuator has been ordered for the two remaining tests, which will allow for testing at frequencies at 2 Hz and above.

5.2 COMPARISON WITH FINITE ELEMENT MODELS (FEM)

The FEM used for sizing the test specimen has been further refined in an effort to match the data obtained during the first fatigue test (Dowd 2001). All FEM were based on a composite model where all the strands and grout, if considered, are modeled as a single equivalent beam. In addition to some modifications to model the loading at mid-span more accurately, the main changes were in the use of uncracked, cracked, and non-grout sections at the anchorage, under the loading point, and along the free length. Table 5-1 shows the 5 models and the different sections used.

Table 5-1: FEM Cross Sections

	Anchorage	Loading Point	Free Length
Model 1	Uncracked	Uncracked	Uncracked
Model 2	No Grout	No Grout	No Grout
Model 3	Tension Zone Cracked	Tension Zone Cracked	Tension Zone Cracked
Model 4	No Grout	Tension Zone Cracked	Tension Zone Cracked
Model 5	No Grout	No Grout	Tension Zone Cracked

Table 5-2 shows the measured and FEM estimated ram force and natural frequency of the test specimen. All of the FEM's overestimate the stiffness of the specimen. The ram force was overestimated by 18% to 30% and the fundamental natural frequency by 13% to 22%. This is also true for the model that completely neglects the grout for the stiffness estimate. The data in Table 5-2 indicate that the FEM needs to be modified, and a different analytical approach might be necessary. However, the FEM solution by Dowd certainly represents an initial approach on which further FEM work should be based.

Table 5-2: Specimen#1, #2 and FEM – Ram Force and Initial Frequency

	Ram Force Range	Frequency
Specimen #1	15.4 kip	N/A
Specimen #2	15.3 kip	12.5 Hz
Model 1	20.0 kip	15.2 Hz
Model 2	18.1 kip	14.1 Hz
Model 3	18.9 kip	14.5 Hz
Model 4	18.7 kip	14.4 Hz
Model 5	18.7 kip	14.4 Hz

The different FEM's also predicted values of stress expected during the test. Validation of the calculated stresses is available by comparing with stress data obtained by measuring strains on the polyethylene and the grout. The strains measured on the polyethylene and the grout have been extrapolated to the failure location on the strand (Dowd 2001). The stresses on the strands estimated from the measured strains were approximately 34 ksi (230 N/mm^2) at the beginning of the test and decreased drastically over the testing period, which may indicate strain gage failures or grout cracking. The calculated FEM stresses at the anchorage varied between 30 ksi and 45 ksi (200 N/mm^2 and 310 N/mm^2) depending on the model used. However, no stresses were measured on the actual strands and the estimated stress data from the strain measurement on the grout and polyethylene contain some degree of uncertainty. Considering the fact that the stiffness of the specimen was overestimated in the FEM, the FEM stress estimates need to be interpreted carefully and further studies are necessary.

5.3 COMPARISON WITH EXISTING FATIGUE DATA

The biggest factor in being able to judge the fatigue behavior of the specimens, and eventually the actual stay cables, are good estimates of the stress range that occur at the failure locations. As shown earlier, the only stress estimates are from FEM's and some experimental validation.

A comparison of the FEM estimated stresses and the number of cycles for which wire breaks occurred at the tower anchorage are shown in an S-N plot in Figure 5-1. The graph shows the mean value of published axial fatigue data, a suggested design equation for strand, the axial fatigue requirement for stay cables, the Japanese bending fatigue test (all discussed in Chapter 1), as well as the results from the two bending fatigue tests. As mentioned before, the lower and upper bound of the stress range from the FEM were between 30 and 45 ksi (200 N/mm^2 and 310 N/mm^2). The first break at the tower anchorage of specimen #1 occurred after 300,000 cycles and the last (14^{th}) after 2,550,000 cycles. The corresponding values for specimen #2 are 420,000 cycles for the first break and 2,800,000 cycles for the last (51^{st}) break. Although the stress range cannot be defined as a single value at this point, the test results compare reasonably well with the existing axial fatigue data.

Note that strain measurements on critical strands have been considered, and attempts to attach strain gages to the strand at locations of interest have been made. However, it was found that obtaining reliable and meaningful strain data from strands is generally very difficult. The use of strain gages on strands is further complicated by the chance of mechanical damage during installation, stressing and grouting. Nevertheless, the use of strain gages should be considered on future specimens.

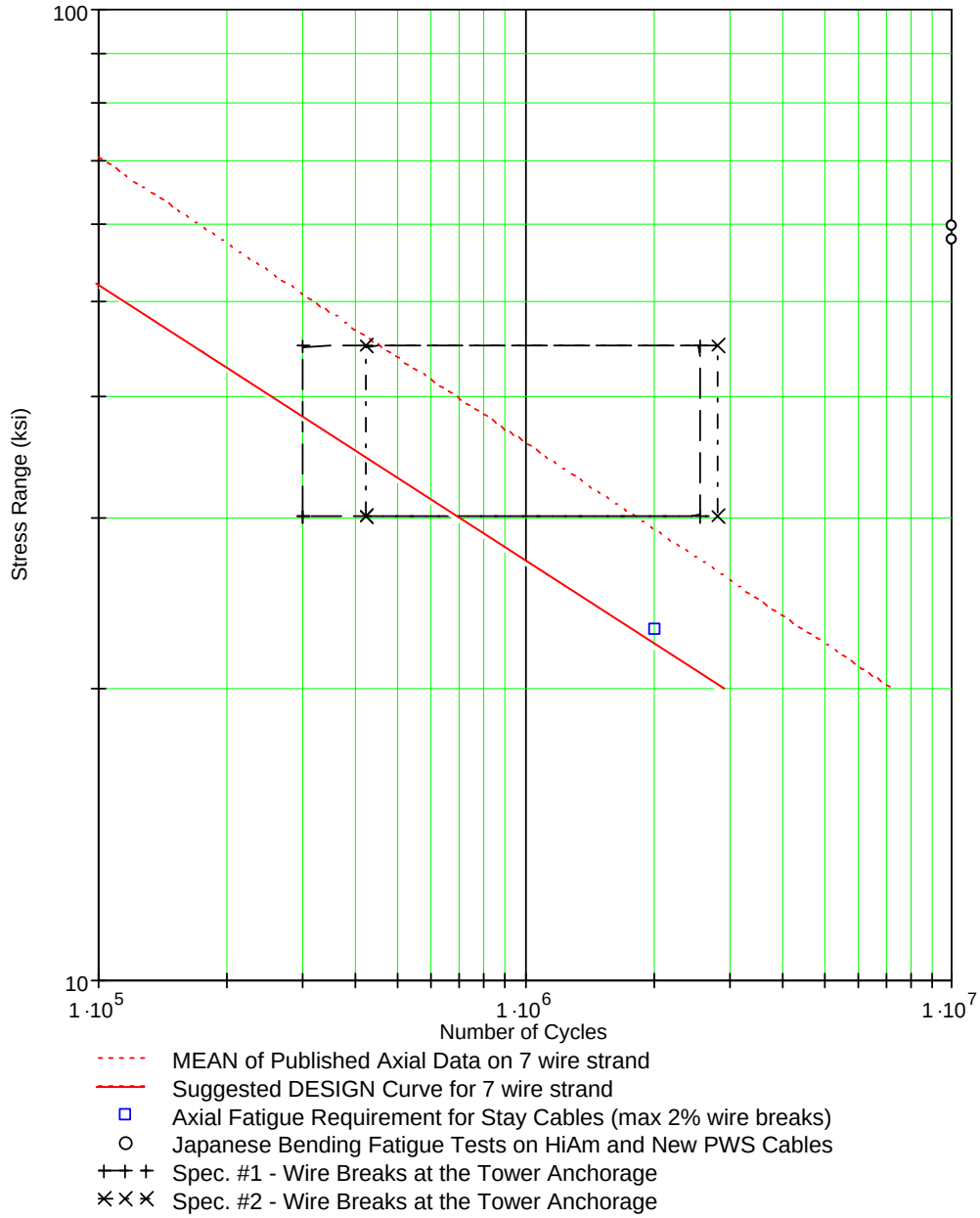

Figure 5-1: Comparison with Existing Fatigue Data

5.4 OUTLOOK

Generally, a fairly large number of tests are required for fatigue-critical details to be able to predict their performance reasonably well. There are still numerous unanswered questions related to fatigue in axially loaded stay cables, although large numbers of tests have been performed. Considering this, the two bending fatigue tests might not be more than a starting point to get a general idea of the behavior. The results of the two tests need to be verified by changing different parameters of the specimen. However, there are a few key points that can be made based on the two tests.

The initial cable design for the Fred Hartman Bridge did not fulfill the necessary anchorage test requirements (Chapter 1). As a result of the 4 tests performed at FSEL in 1989, one extra strand was added to all stay cables for the actual design of the Fred Hartman Bridge. No further tests were performed to validate this measure, which leaves numerous open questions on the durability and actual performance of the stay cables. This is of special concern because it is obvious after the two bending fatigue tests that the large amplitude stay cable vibrations might play a very important role in the overall fatigue performance of the stay cables. Visually, it appeared that the maximum amplitudes that occurred at the anchorage of the actual cables during a vibration event might have been larger than the amplitudes that occur during the testing.

Table 5-3 shows hours of continuous cable vibration required at different frequencies until the first wire break occurred. The numbers of cycles to the first wire break are based on the two fatigue tests. The frequencies of 1 to 3 Hz represent the dominant frequencies of wind and rain induced vibration events (Chapter 1). Some of the FEM estimated a stress range of up to 70 ksi (470 N/mm^2) on actual bridge cables during large vibration events (Dowd 2001). Assuming that the stress range that occurred at the anchorage on the two

specimens was 35 ksi (235 N/mm^2) (see also Section 5.2), one can estimate the number of cycles and hours of continuous cable vibration required for the first wire break to occur at a stress range of 70 ksi (470 N/mm^2). Note that this simplified transformation assumes that the fatigue life follows the equation commonly used for structural steel. The equation use is given below:

$$N_2 = N_1 \cdot \left(\frac{\Delta\sigma_1}{\Delta\sigma_2} \right)^3$$

Table 5-3: Hours of Continuous Vibration – Specimen #1 & #2

Estimated Stress Range at the Anchorage: 35 ksi

Cycles	Remark	1 Hz	2 Hz	3 Hz
300,000	1st break specimen #1	83 hrs	42 hrs	21 hrs
420,000	1st break specimen #2	117 hrs	58 hrs	29 hrs

Table 5-4: Hours of Continuous Vibration – Stay Cables

Estimated Stress Range at the Anchorage: 70 ksi

Cycles	Remark	1 Hz	2 Hz	3 Hz
37,500	Corresponding: 1st break specimen #1	10 hrs	5 hrs	3 hrs
52,500	Corresponding: 1st break specimen #2	15 hrs	7 hrs	4 hrs

Considering the relatively low bounds of 3 hours to 117 hours of continuous cable vibration, fatigue damage may already have occurred. However, it is not possible at this point to predict the extent of the fatigue damage more reliably because the correlation between the FEM and the specimen is too poor to project the test results to an actual stay cable.

The rate of occurrence of the wire breaks on the specimens indicates that the actual stays might have enough redundancy so that once wire fractures start to occur, enough time remains to take the appropriate actions. However, this implies that means available to detect wire breaks on the actual bridge cables are reliable. The acoustic monitoring system (Soundprint) used for the fatigue tests, appeared to be very reliable and might be one of the possible solutions for a permanent monitoring of the actual stay cables.

It appeared from the two tests that there might be some interaction between the strand and grout which is not favorable for the fatigue life. The fact that all the failures occurred at the tower anchorage, which was the top end during the grouting operation, might be an indication that the grout influences the behavior of the strands differently along the length. Looking at earlier research on stay cables (Hamilton 1995) indicates that the behavior of the grout is not fully understood, which calls for further investigations. Note that the grout is meant to protect the strands from corrosion. Considering the importance of corrosion protection, one would wish that there were specifications that control the grout quality, as well as the grouting operation.

Furthermore, the influence of corrosion on the fatigue life of strands and the anchorage has not been studied. No serious corrosion was observed on the strands or the anchorage in the two tests. However, the observed exposed strands in the grout void (Chapter 4) indicate that there are locations that are very susceptible to corrosion. Note that there are numerous reports of heavily corroded strands and anchorages in anchorage tests (Chapter 1) that have never been completely resolved.

Based on the knowledge from the two fatigue tests, it is recommended that the actual stay cables are closely monitored and the bending fatigue behavior is further investigated. Of special interest in terms of fatigue is the behavior of

specimens with different sizes, at different amplitudes, and the interaction between grout and strand. In addition, the influence of imperfections such as crossed strands, grout voids, grout cracking, and exposed strands and anchorages are to be studied. On the analytical side, models are required that have better correlation with experimental data to be able to project experimental data to actual stay cables.